ASIAN JOURNAL OF ELECTRICAL AND ELECTRONIC ENGINEERING

AIMS & SCOPE OF THE ASIAN JOURNAL OF ELECTRICAL AND ELECTRONIC ENGINEERING

The **Asian Journal of Electrical and Electronic Engineering** (AJoEEE), published biannually (March and September), is a peer-reviewed open-access journal of the **AlamBiblio Press**.

The Asian Journal of Electrical and Electronic Engineering publishes original research findings as regular papers and review papers (by invitation). The Journal provides a platform for Engineers, Researchers, Academicians, and Practitioners who are highly motivated to contribute to the Electrical and Electronics Engineering disciplines. It also welcomes contributions that address the developing world's specific challenges and address science and technology issues from a multidisciplinary perspective.

REFEREES' NETWORK

All papers submitted to AJoEEE Journal will be subjected to a rigorous reviewing process through a worldwide network of specialized and competent referees. Each accepted paper should have at least two positive referees' assessments.

SUBMISSION OF A MANUSCRIPT

A manuscript should be submitted online to the Asian Journal of Electrical and Electronic Engineering (AJoEEE) website https://alambiblio.com/ojs/index.php/ajoeee. Further correspondence on the status of the paper could be done through the journal website

ASIAN JOURNAL OF ELECTRICAL AND ELECTRONIC ENGINEERING

ASIAN JOURNAL OF ELECTRICAL AND ELECTRONIC ENGINEERING

eISSN 2785-8189

9 772785 818002

Whilst the publisher and editorial board make every effort to see that no inaccurate or misleading data, opinion or statement appears in this Journal, they wish to make it clear that the data and opinions appearing in the articles and advertisements herein are the responsibility of the contributor or advertiser concerned. Accordingly, the publisher and the editorial committee accept no liability whatsoever for the consequence of any such inaccurate or misleading data, opinion or statement.

ASIAN JOURNAL OF ELECTRICAL AND ELECTRONIC ENGINEERING

Volume 3, Issue 2, September 2023

TABLE OF CONTENTS

Performance Analysis of Different Grid Substations with Demand-Side-Management-Based Optimal Power Usage

Farhad Uddin[1], Dilip Kumar Tripura[2], and Syed Munimus Salam[*2],
Muhammad Mahbubur Rashid[3]

[1,2]*Dept. of EEE, Southern University, Chattagram, Bangladesh*
[*2]*Dept. of EEE, USTC, Chattagram, Bangladesh*
[3]*Department of Mechatronics, Faculty of Engineering, International Islamic University Malaysia*

*Corresponding author: munim53@gmail.com

Abstract— This study is centered on analyzing the performance of two power grid stations in the southern grid zone of Bangladesh. Additionally, it encompasses the effect of a demand-side management simulation of grid line operation. Firstly, this paper briefly discusses the grid circle's interconnected grid system and the serving districts' generation capacity. An analysis of schematic diagrams and an examination of the current substations and transmission cables in place has been conducted. The maximum load research has been addressed at several significant grid sub-stations, examining the capacity of a specific grid zone and determining the necessity for expanding the corresponding grid infrastructure. This study presents a comprehensive analysis of the DSM employed in the grid substation, as well as an examination of the various possibilities of renewable energy installations within it. Additionally, this study encompasses the investigation of power transmission and the accompanying structures employed for transmission, as well as the analysis of the estimation technique and any other interconnected domains.

Keywords: *Power grid, Simulation, and Renewable energy.*

1. INTRODUCTION

The Power Grid Business of Bangladesh (PGCB) is a government-owned electric utility business based in Dhaka, Bangladesh. It is one of the largest entities in the field of Power Transmission utilities. The Power Grid is crucial in facilitating the expansion of Bangladesh's power sector by establishing a strong and integrated national grid. Additionally, it is actively involved in the government's flagship initiative aimed at ensuring universal access to electricity. Advancement in the field of Technical and management has led to the synchronized progress of power transmission networks and the efficient operation and management of regional and national grids. POWERGRID, in its capacity as the Central Transmission Utility of the nation, is significantly contributing to the development of the power sector in Bangladesh and facilitating Open Access to its inter-state transmission system. POWERGRID has formulated a strategic plan to establish a robust and dynamic national grid throughout the country, implementing it systematically and gradually. This approach aims to maximize the efficient exploitation of generating resources, preserve environmentally sensitive areas along the transmission route, and handle the inherent unpredictability associated with power generation facilities. The enhancement of the National Grid is being strategically implemented through a systematic approach that involves the consolidation of the inter-regional link architecture [1].

In this scholarly article, the authors introduce a novel metric referred to as the power grid transmission performance index (PI) [2]. This index facilitates the explanation of several conventional power grid transfer issues, including the assessment of transfer capabilities, coordination among power plants, power grid and loads, and the evaluation of power grid capacity margin. This article addresses the issue of electricity transmission systems in the Chattogram Zone, as discussed in reference [3]. This discussion briefly addresses the

interconnected grid system within the Chattogram circle and the generation capability of the Chattogram districts. We have conducted an examination of schematic diagrams, pre-existing sub-stations, the protection mechanism, and the current transmission lines. We have also examined the maximum load analysis conducted on significant sub-stations, as well as the peak hour demands seen in various grid sub-stations. To showcase the capabilities of the Simulink transmission line simulator, we will now examine a number of renowned instances [4]. The phenomena encompassed in this category consist of the propagation of waves and the dependence of velocity on the numerical values of the elements.

Furthermore, we shall examine the concept of reflection occurring at a linear terminating impedance. The phenomenon of pulse dispersion will be demonstrated. In this section, we will now discuss the concept of reflection occurring at a nonlinear terminating impedance. In this thesis, titled "Study of Patna 400/220 KV Substation," the focus is on the Power Grid Corporation Of India Limited [5]. This work introduces a MATLAB/Simulink model of a multiagent system designed to automate transmission utilities in order to mitigate grid outages. The model is presented in [6]. This study introduces the design and modeling of a Distance relay using the MATLAB/SIMULINK software, as documented in reference [7]. A transmission line network has been constructed, and fault voltages and currents resulting from both symmetrical and unsymmetrical faults have been graphed. During fault conditions, the transmission line network experiences an input voltage and current that comprise DC offset values and higher-order harmonics.

Demand-side management is a crucial component of power delivery networks' energy management systems, as it enables users to exercise control over their load consumption patterns [7]. The alteration of the electric load consumption profile can be achieved by one of four approaches. The impact of energy efficiency extends beyond peak usage periods, as it leads to a decrease in overall energy consumption. The analysis of efficiency improvement is further examined in the studies conducted by Chowdhury et al. (2018) [8] and Tronchin et al. (2018) [9]. The concept of time of use refers to a billing strategy that involves charging consumers varying rates based on their energy usage habits during different periods of the day [10],[11]. The proposed approach consists of the segmentation of fixed utility prices into several temporal intervals spanning a 24-hour duration. The utilization of differential tariffs for electricity units can potentially mitigate the effects of peak load rates and seasonal fluctuations in pricing tariffs. Rebours and Kirschen (2005) [12-16] posit that in instances where there is an unanticipated decline in electricity generation, the spinning reserve of the electric grid system can be mobilized by the distribution network operator (DNO) to compensate for the disparity between consumption and generation. Demand response, in the context of the electricity wholesale market, occurs when end-user consumers deviate from their typical load consumption patterns in response to changes in unit tariffs over time or as a result of incentivized programs aimed at reducing load consumption. This phenomenon is particularly relevant during periods of high tariffs or when grid stability is compromised [17-19].

2. PROBLEM FORMULATION

It is imperative to accurately simulate each regular load utilized by residential, semi-industrial, and industrial consumers in order to enhance the efficiency and reliability of the power grid system. Following the process of load-modeling and categorization, there exist two distinct methodologies for determining the load combination.

The top-down approach is a methodology that involves starting with a broad perspective and then gradually narrowing down to specific details or components.

The bottom-up technique is a methodology that involves starting with specific details or elements and gradually building up to a more extensive, more comprehensive understanding or conclusion.

Top-down methodologies are employed with the fundamental objective of consolidating all power consumption units inside a given unit. Consequently, this strategy only provides information on the overall energy consumption of a specific geographical region [14]. In contrast to the top-down approach, the bottom-up methodology examines the individual power consumption of each appliance in isolation. The regular load curve for a base station or multiple base stations can be easily obtained by aggregating the consumption of all devices [15]. In order to determine the hourly energy usage, historical data is utilized employing a bottom-up technique for various appliances over the course of a whole day.

Uddin et al.

2.1 Illustrations of Load Profile

The load consists of residential, industrial, and commercial components under typical user-defined conditions. To facilitate load modeling, extraneous parameters are omitted in order to establish a streamlined calculation model. In the context of load analysis, template base shapes are typically employed for nonlinear loads, while linear loads are represented by regular shapes that incorporate the power factor. For example, an industrial inductive load such as a ventilation system exhibits a power factor variation distinct from that of resistive loads inside the power grid. The home load has a consumption profile characterized by a certain power factor.

The proposed methodology involves conducting a periodic survey to assess the bottom-up load calculation approach for various customer types. The appliances are categorized based on their ability to be shifted and further divided into three groups: 1) Thermostatically controlled loads (TCL), which are specifically related to air conditioning units for base stations; 2) Lighting loads (LL), which can be adjusted to different periods based on comfort and economic factors; and 3) Household loads (HL), encompassing appliances such as washing machines, cookers, pumps, and monitoring computer terminals, which are essential for providing basic services.

2.1.1. Calculation by Demand Side Management

There are two stages of DSM energy calculation in the Grid Network. At first, the system energy calculation includes three factors: the load profile of used loads by the users, the class of the users covered by the system model, and the environmental and timing issues that affect the uses of the load data. Secondly, a simplified model of the grid model is used to produce electrical power calculation with and without DR following a linear relationship with the load models. The output calculation expressed the power saving of a grid network using the bulk amount of load in a particular test grid system. Different test grids like six, fourteen and higher number of nodes with IEEE test bus system are utilized to get the system output.

For a typical load modeling scenario, Considering N_T samples in a capture period, the acquired samples are sequences of length N_T as shown in (1) and (2).

$$v_{load} = \{v_{load}(n)\}_{n=1}^{N_T} \qquad (1)$$

$$i_{load} = \{i_{load}(n)\}_{n=1}^{N_T} \qquad (2)$$

The energy consumption for any load number can be obtained from

$$P_{load} = \frac{1}{N}\sum_{n=1}^{N} v_{load}(n)i_{load}(n) \qquad (3)$$

For load modeling purposes, assuming the temperature control loads (TCL) as a different category. As these loads depend on temperature for consuming power. 'P_{TCL_load}' suitable modeling equation can be expressed as,

$$N_{TCL\_load} = \begin{cases} 0 & temp \leq lower\_threshold \\ 1 & temp \geq upper\_threshold \\ N_{TCL\_load} = condition\ of\ TCL\ load \end{cases} \qquad (4)$$

and

$$P_{TCL\_load} = \frac{1}{N}\sum_{n=1}^{N} N_{TCL\_load} * v_{load}(n)i_{load}(n) \qquad (5)$$

Shiftable loads can be considered as loads that can be shiftable to another time period, like washing machines, water pumps, telecom rectifiers, etc. As a result, the energy demand at this time will be reduced by the energy that would have been consumed by it. These loads depend on the time period for consuming power 'P_{FL_load}' suitable modeling equation can be expressed as,

$$N_{FL\_load} = \begin{cases} 0 & time \leq lower\_threshold \\ 1 & time \geq upper\_threshold \\ N_{TCL\_load} = condition\ of\ TCL\ load \end{cases} \qquad (6)$$

and

$$P_{FL\_load} = \frac{1}{N}\sum_{n=1}^{N} N_{FL\_load} * v_{load}(n)i_{load}(n) \qquad (7)$$

Thus, considering base load as 'P_{BL_load}' and thus total active power '$P_{Total\_load}^k$' can be calculated for 'k' time period,

$$P_{Total\_load}^k = P_{BL\_load}^k + P_{FL\_load}^k + P_{TCL\_load}^k \qquad (8)$$

Similarly, we can consider '$Q_{Total\_load}^k$' as total reactive power for 'k' time period,

$$Q_{Total\_load}^k = Q_{BL\_load}^k + Q_{FL\_load}^k + Q_{TCL\_load}^k \qquad (9)$$

If any aggregator is responsible for coordinating at 'l 'number of loads in a power network then,

$$P_D^k = \sum_{L=1}^{l} P_{Total\_load}^{k,L} \qquad (10)$$

and

$$Q_D^k = \sum_{L=1}^{l} Q_{Total\_load}^{k,L} \qquad (11)$$

The standard version of AC optimal power flow, the power balance equation expressed as functions of the voltage angles 'θ^k' and magnitudes 'V_m^k' and generator injections 'P_g^k' and 'Q_g^k', where the load injections are assumed constant and given:

Here, the objective function for the power grid network with n_g generator is

$$minmize \quad \sum_{i=1}^{n_g} f_P^{i,k}\left(P_g^{i,k}\right) + f_Q^{i,k}\left(Q_g^{i,k}\right) \qquad (12)$$

Subject to

$$g_p\left(\theta^k, V_m^{\ k}, P_g^{\ k}\right) = P_{bus}\left(\theta^k, V_m^{\ k}\right) + P_D^k - C_g^k P_g^k = 0 \qquad (13)$$

$$g_p\left(\theta^k, V_m^{\ k}, Q_g^{\ k}\right) = Q_{bus}\left(\theta^k, V_m^{\ k}\right) + Q_D^k - C_g^k Q_g^k = 0 \qquad (14)$$

Where '$f_P^{i,k}$' and '$f_Q^{i,k}$' are the cost functions of real and reactive power injections in a sparse ($nb \times ng$) generator connection matrix Cg can be defined such that its (i, j) th element is 1 if generator j is located at bus i and 0 otherwise. Also subject to the inequality constraints $h\left(\theta^k, V_m^{\ k}\right)$ are the branch flow limits and the minimum and maximum values. Bounding condition includes reference bus angles, voltage magnitudes and generator injections.

3. METHODOLOGY

The proliferation of electrical and electronics loads in residential dwellings, commercial complexes, and office spaces has experienced a significant surge within the last two decades. These particular categories of loads have contributed to an improvement in the overall quality of life and have resulted in an increased use of electrical power. Both electrical and electronic equipment require higher power supplies as they are designed for decentralized networks. With the growing demand for energy, there is a need for stricter infrastructure support to accommodate the supply of electrical energy. The majority of power supplies are engineered to fulfill requirements related to regulated output, isolation, and compatibility with diverse grid systems. The load type and electricity usage exhibit variability across different localities. The usage of domestic energy has experienced a steady increase throughout time. The predominant portion of home electrical energy is utilized for the purposes of illuminating spaces and operating cooling fans. The majority of residential loads have a single-phase characteristic and receive power from single-phase mains. By utilizing load templates, it becomes feasible to assess the influence of various categories of residential loads on a distributed system. By employing template-based load modeling, it becomes feasible to ascertain the system's power consumption, voltage, power factor (PF), and energy need for any given number of loads within a feeder [18].

The calculation of an output load is possible for user-defined load combinations, which can then be applied to

the node bus of various bus systems, such as the six or fourteen-test bus system provided by the Institute of Electrical and Electronics Engineers (IEEE). Figure 1 illustrates that when the system load is substituted with a percentage, there is a reduction in output consumption. Ultimately, the diminished computed load is employed to obtain an optimal power flow (OPF) solution for the system.
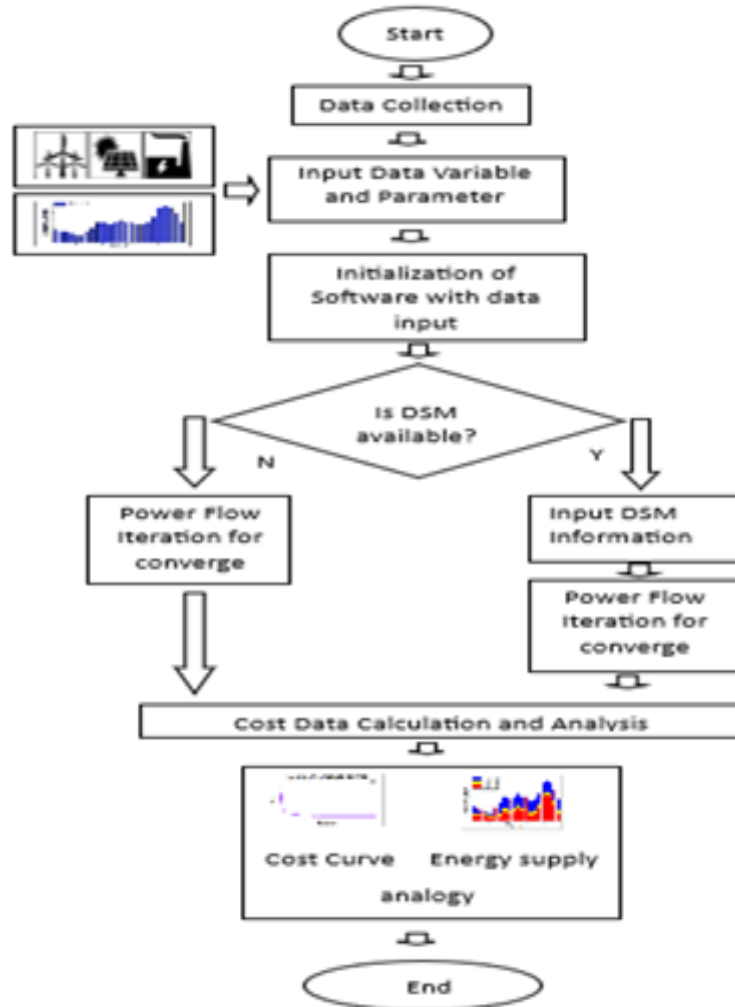
Figure 1: Flow chart of the proposed system

4. RESULT AND DISCUSSION

A comparison analysis was conducted to examine the power consumption of individuals within 24 hours, measured in megawatts (MW), for the grid system under investigation. The general pattern exhibits fluctuations with a small upward trajectory toward the conclusion of the observed timeframe. The electricity consumption in the considered region initially begins at a level just below 140MW and fluctuates within a range of approximately 140MW to 120MW throughout the subsequent eight hours. The consumption demand experienced significant fluctuations, reaching a peak of 180MW at 20:00. Subsequently, there was a decline in power utilization throughout the early hours of the night, namely during four hours, resulting in a reduction of 160 megawatts.

However, it should be noted that the power consumption demand remained slightly below 80MW within the specified timeframe. Subsequently, there was a marginal decrease in the consumption of load demand within the subsequent 8-hour period. Subsequently, there was a gradual increase in the load demand, with a progressive decrease and subsequent increase to a maximum of 18.30 below 100MW. Ultimately, the level of consumption had a consistent decline, reaching a value of 80MW.

Figure 2: Load curve of the nodes collected from PGCB

The line graph of Figure 3 illustrates the power consumption of the monthly load curve, measured in megawatts (MW). The entire demand for power consumption exhibited significant fluctuations and experienced a drop.
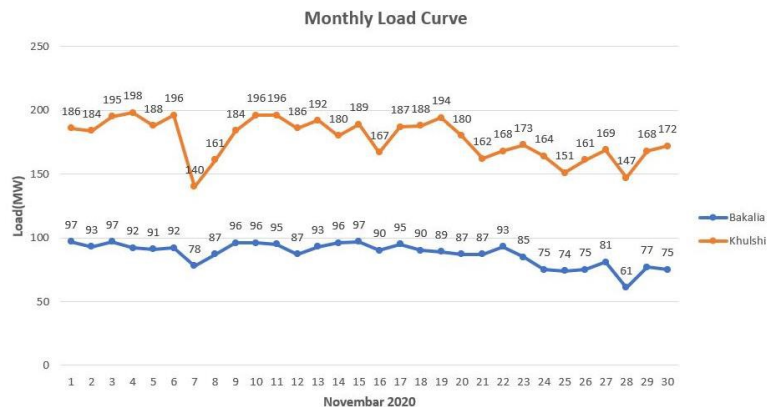
Figure 3: One-month load curve for the considered system

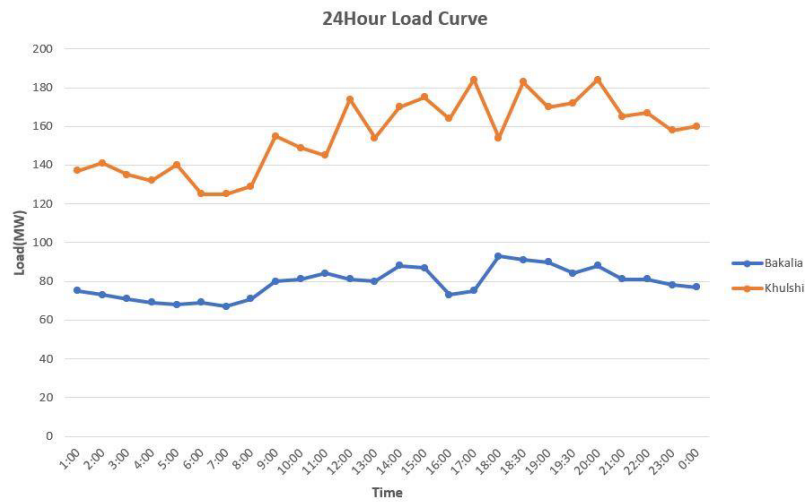The initial power output at Khulshi was recorded at 186MW, followed by minor fluctuations over the subsequent five days, reaching a peak of 196MW and seeing tiny increases and decreases over this period. Subsequently, the load demand exhibited a sharp increase, reaching a value of 140 during the subsequent two days. Following a period of continuous growth in 196, the data subsequently stabilized in the subsequent days. The demand for consumption exhibited significant fluctuations during the whole day, reaching a peak of 172MW.

On the contrary, the consumption load commenced at 97MW within the specified time period. Subsequently, the load demand exhibits a consistent decrease over a period of seven days, reaching a value of 78MW. Subsequently, there was a gradual increase in the load demand, which eventually stabilized over a period of 22 days at a level of 93 MW. The load saw a gradual decrease and afterward exhibited fluctuations, reaching a maximum of 75MW in recent days.

The production cost of the test grid system is consistently decreased for all levels of load demands. Figures 8 a, b, c, and d display the hourly production of the Distributed Energy Resources (DERs) for the schemes with 5% Demand Side Management (DSM), 10% DSM, and 15% DSM, respectively. It is important to acknowledge that the hourly output of the grid heavily impacts the decrease in grid production costs. The implementation of grid control mechanisms results in a reduction in production expenses associated with power usage.

Uddin et al.
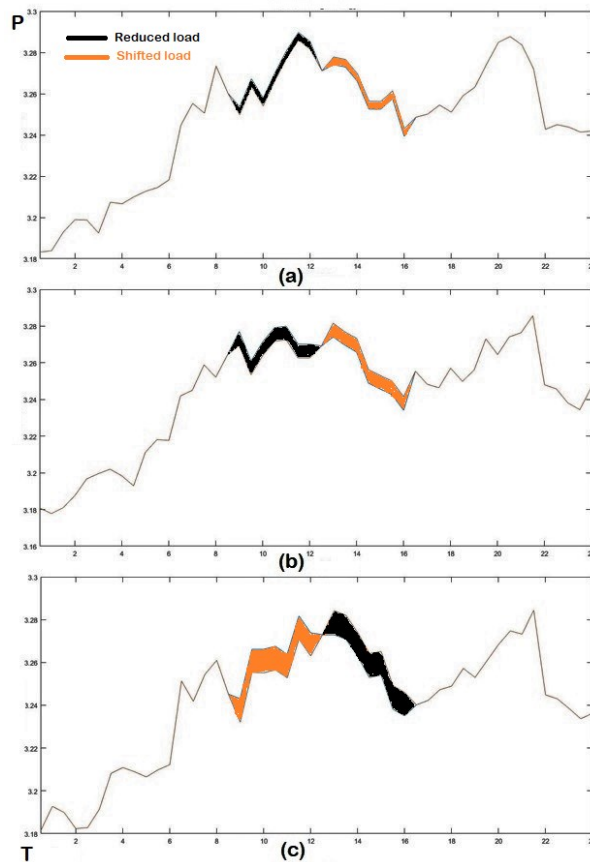
Figure 4: Load shifting for DSM (a 5%, b 10%, c15%)

The implementation of time-of-use (TOU) energy market pricing, which incentivizes aggregators to sell electricity to customers while offering certain compensation, is believed to have an impact on grid demand. The remaining distributed energy resources (DERs) will be adequate to modify the overall load demand of the test grid system inside this specific hour.

In order to examine the impact of the FL load shift, the calculation of the minimum generation cost is conducted without accounting for LL and TCL. The omission of the Firm Load (FL) in the grid system results in a substantial escalation in the expenditure associated with generating one hour's worth of production. The cost experiences a reduction when the aspect of moving is taken into account. As a result of the evolving role of the grid and the examination of cost generation across four separate Demand-Side Management (DSM) strategies, it is deemed unnecessary for the grid to get energy from high-cost production sources.

TABLE I: DEMAND CHARACTERISTICS

	Without DSM	5% reduction	10% reduction	15% reduction
Peak	3.2843	3.272	3.271	3.267
AVG	2.2421	2.2420	2.2417	2.2416
Peak Reduction (%)		0.09	0.27	0.65
Load factor	0.6826	0.6828	0.6831	0.6838

On the other side, Figure 4's b and c depict the possibility of an alternative peak, which might raise the cost of production in comparison to Case 1. The grid's best strategy for transferring grid users is to utilize a TOU-based power market pricing model, according to a comparison of prices in Figure 10. In this case, the grid controls the market price of power, allowing customers to maintain their standard of living while perhaps lowering prices overall.

5. CONCLUSION

In summary, enhancing active grid involvement is crucial for mitigating the generation costs of the system. The costs associated with electricity generation exhibit similarity when compared with the implementation of Demand Side Management (DSM), resulting in a cost reduction ranging from 15% to 31% compared to the costs obtained without DSM. Moreover, DSM offers several advantages, such as reducing peak demand and increasing the load factor while simultaneously managing the total load and average load of the demand. The efficiency of demand-side management (DSM) relies on the incorporation of both time-of-use (TOU) and incentive-based power market pricing. Consequently, the cost of energy must vary on an hourly basis in accordance with the prevailing demand. The influence of the fixed electricity price on demand-side management (DSM) load modeling is minimal. The costs associated with the generation of the system increase when the grid price is decided.

REFERENCES

[1]   J. Carpentier, "Optimal power flows," Int. J. Electr. Power Energy Syst., vol. 1, no. 1, pp. 3–15, 1979, doi: 10.1016/0142-0615(79)90026-7.

[2]   A. M. Al-Shaalan, "Reliability Evaluation of Power Systems," in Reliability and Maintenance - An Overview of Cases, IntechOpen, 2020.

[4]   IEA, "World Energy Outlook 2020," 2020. [Online]. Available: https://www.iea.org/reports/world-energy-outlook-2020.

[5]   J. Martínez-Lao, F. G. Montoya, M. G. Montoya, and F. Manzano-Agugliaro, "Electric vehicles in Spain: An overview of charging systems," Renew. Sustain. Energy Rev., vol. 77, pp. 970–983, Sep. 2017, doi: 10.1016/j.rser.2016.11.239.

[6]   S. Saini, "Conservation v. generation," Refocus, vol. 5, no. 3, pp. 52–54, May 2004, doi: 10.1016/S1471-0846(04)00146-5.

[7]   S. M. Salam, N. Mohammad, S. Barua, and M. I. Uddin, "A Comprehensive Analysis of Power Grid with IEEE 14 Bus System Model for Deregulated Compatibility of an Isolated Grid," 2021, vol. 2021, pp. 12–13.

[8]   K. B. H. J. B. E. Daalder, Operation of Restructured Power Systems the Kluwer International Series. 2001.

[9]   R. Lu, S. H. Hong, and X. Zhang, "A Dynamic pricing demand response algorithm for smart grid: Reinforcement learning approach," Appl. Energy, vol. 220, pp. 220–230, Jun. 2018, doi: 10.1016/j.apenergy.2018.03.072.

[10]   S. Nan, M. Zhou, and G. Li, "Optimal residential community demand response scheduling in smart grid," Appl. Energy, vol. 210, pp. 1280–1289, Jan. 2018, doi: 10.1016/j.apenergy.2017.06.066.

[11]   C. Bergaentzlé, C. Clastres, and H. Khalfallah, "Demand-side management and European environmental and energy goals: An optimal complementary approach," Energy Policy, vol. 67, pp. 858–869, Apr. 2014, doi: 10.1016/j.enpol.2013.12.008.

[12]   M. Hildmann, A. Ulbig, and G. Andersson, "Empirical Analysis of the Merit-Order Effect and the Missing Money Problem in Power Markets With High RES Shares," IEEE Trans. Power Syst., vol. 30, no. 3, pp. 1560–1570, May 2015, doi: 10.1109/TPWRS.2015.2412376.

[13]   S. M. Salam, M. J. Uddin, and S. Hannan, "A new approach to develop a template based load model that can dynamically adopt different types of nonlinear loads," in 2017 International Conference on Electrical, Computer and Communication Engineering (ECCE), Feb. 2017, pp. 708–712, doi: 10.1109/ECACE.2017.7912996.

[14] S. M. Salam and N. Mohammad, "Load Flow Analysis of a Six Bus System for a Bulk Scale Replacement of Conventional Lighting Loads in a Distributed Network," in 2020 IEEE Region 10 Symposium, TENSYMP 2020, 2020, no. June, pp. 831–834, doi: 10.1109/TENSYMP50017.2020.9230818.

[15] X. Lu et al., "Optimal Bidding Strategy of Demand Response Aggregator Based on Customers Responsiveness Behaviors Modeling under Different Incentives," IEEE Trans. Ind. Appl., vol. 9994, no. c, 2021, doi: 10.1109/TIA.2021.3076139.

[16] S. M. Salam and N. Mohammad, "Analyze the Impact of Demand Side Management on Grid Power for an Isolate Zone in a Sustainable IEEE 14 Bus System," 2021 Int. Conf. Inf. Commun. Technol. Sustain. Dev. ICICT4SD 2021 - Proc., pp. 16–20, 2021, doi: 10.1109/ICICT4SD50815.2021.9396975.

[17] F. Wang et al., "Day-ahead optimal bidding and scheduling strategies for DER aggregator considering responsive uncertainty under real-time pricing," Energy, vol. 213, p. 118765, Dec. 2020, doi: 10.1016/j.energy.2020.118765.

[18] S. D. Manshadi and M. Khodayar, "A hierarchical electricity market structure for the smart grid paradigm," in 2016 IEEE Power and Energy Society General Meeting (PESGM), Jul. 2016, pp. 1–1, doi: 10.1109/PESGM.2016.7741852.

[19] C. Heinrich, C. Ziras, A. L. A. Syrri, and H. W. Bindner, "EcoGrid 2.0: A large-scale field trial of a local flexibility market," Appl. Energy, vol. 261, p. 114399, Mar. 2020, doi: 10.1016/j.apenergy.2019.114399.

Investigation of a Polymer-based SAW Sensor to Detect Volatile Organic Compound (VOC)

Nur Fatin Nabilah Mohamad Sabri, Nor F. Za'bah*, and Aliza Aini Md Ralib

Department of Electrical and Computer Engineering, Kulliyyah of Engineering, International Islamic University Malaysia, Kuala Lumpur

Corresponding author: adah510@iium.edu.my

Abstract— Two surface acoustic wave (SAW) sensors with polyethyleneimine (PEI) and polyisobutylene (PIB) layers respectively are modelled by using COMSOL Multiphysics software to detect acetone, benzene, and toluene. The main parameter of the SAW sensor is the thickness of the sensing layer, and the concentration of VOCs is varied to study their relationships with regard to the sensitivity of the SAW sensor. Both configurations portrayed the same pattern where the frequency shift and the sensitivity increase as the concentration of VOCs increases. In addition, the two layers have also produced promising results in sensing toluene even as low as 5 ppm which means that both layers are more selective towards toluene when the three VOCs are concurrently presented on the surface of the sensor. The data also shows that in detecting acetone and benzene, the PEI layer showed higher shifts in frequencies as compared to the PIB layer.

1. INTRODUCTION

There has been a growing interest in investigating second and third hand smoke exposure. This is done by detecting the components in the smoke itself, particularly the volatile organic compounds (VOCs) such as acetone, benzene, and toluene. Second-hand smoke comes from tobacco that sticks on the cloth or hair during active smoking [1]. While third-hand smoke is the excess contamination from tobacco that remains after the cigarette has been put out [1].

Acetone, benzene, and toluene can be detected using commercially available sensors such as pellistor sensor [2]. The sensor detects VOCs by diffusing a mixture of air and VOCs through a porous sensor surface [4]. The porous sensor's main element is a coil made from platinum wire [2]. However, the main problem with this type of sensor is it needs to be heated up to hundreds of degrees by allowing the electric current to pass through the platinum wire [2]. Thus, this sensor is not suitable to be used at room temperature. Another type of sensor that can detect VOCs at room temperature is the SAW sensor, which uses a sensing layer such as metal oxides, polymers, and carbon nanotubes [1, 2]. However, in comparison with polymers, the sensitivity of metal oxides is low at room temperature, and they may exhibit a very long recovery time due to the involvement of redox reactions unlike polymers that generally absorb the gases via physisorption [2]. In addition, a SAW sensor with a metal oxide layer needs to operate at a high temperature environment to react with the gases [2]. Therefore, this paper will focus on simulating a SAW sensor using polymer as the sensing layer and its sensitivity and selectivity will be investigated by varying the relevant parameters such as the thickness of the polymer layer and the concentration of the VOCs.

1.1 SAW Sensor

Fig. 1 shows an illustration of a SAW sensor that includes an interdigital transducer (IDT), piezoelectric substrate and the sensing layer. In order to produce a SAW oscillator configuration, the sensor is connected in a high frequency amplifier feedback loop together with a phase compensation network [3]. The targeted analyte passes through an area between a pair of IDTs, a sensitive region covered with a sensing layer [4]. Once the analyte passes through the region, the sensing layer absorbs the targeted analyte which causes changes in elastic modulus, density, and thickness of the sensing layer [5]. The changes that occur to the sensing layer will change the acoustic wave velocity, which is measured in frequency shift [3, 6]. The frequency variation depends on the concentration

of the targeted analyte. In addition, the targeted analyte also determines whether it is a positive frequency shift or a negative frequency shift. A positive frequency shift occurs because of mass loading while elastic loading causes a negative frequency shift [3].
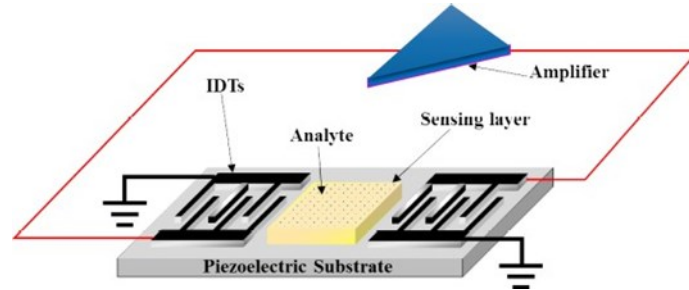

Fig. 1. An illustration of a SAW sensor detecting an analyte [3]

The frequency shift of the SAW oscillator because of mass loading can be calculated using Eq. (1) where k_1 and k_2 are constants of the piezoelectric substrate, h is the thickness of the sensing layer, f_0 is the unperturbed resonant frequency of SAW oscillator, Δm is mass loading and A is the area of sensing film [3, 7].

$$\Delta f = (k_1 + k_2)\, f_0{}^2\, (\Delta m/A) = (k_1 + k_2)\, f_0\, h\, k\, C_v \tag{1}$$

The sensitivity of the SAW sensor towards the targeted analyte is also an important parameter to be investigated. In a SAW sensor, the sensitivity can be calculated using Eq. (2) where Δc is change of analyte concentration and can be expressed as Hz/ppm or Hz/vol [2, 8].

$$S = \frac{\Delta f}{\Delta c} \tag{2}$$

2. METHODOLOGY

There are three main elements in designing a SAW sensor: the sensor's configuration, the piezoelectric substrate, and the sensing layer. There are two types of SAW sensors which are delay lines configuration and resonator configuration. Thus, this work uses the resonator configuration as it is more stable and produces less noise than the delay lines configuration. Secondly, YZ lithium niobate and ST-X quartz are widely used as piezoelectric substrates. This work proposed to use YZ lithium niobate as the material of piezoelectric substrate as it has higher wave velocity than ST-X quartz. Thirdly, the sensing layers that can be used with the sensor include polymer, metal oxides and carbon nanotubes. For this work, two types of polymers are used: polyethyleneimine (PEI) and polyisobutylene (PIB).

Next, the analytes that will be tested in this work are acetone, benzene, and toluene. These VOCs are the main components in second and third hand smoke.

2.1 Configuration in COMSOL

Fig.2 shows the detailed steps to model and simulate the SAW sensor using COMSOL Multiphysics software. Initially, the modelling of the VOCs requires five parameters which are:

    i.   concentration of the VOCs in ppm
   ii.   concentration of the VOCs in the air
  iii.   the molar mass of the VOCs (shown in Table 1)
  iv.   air partition constant for the VOCs in the polymers (shown in Table 1)
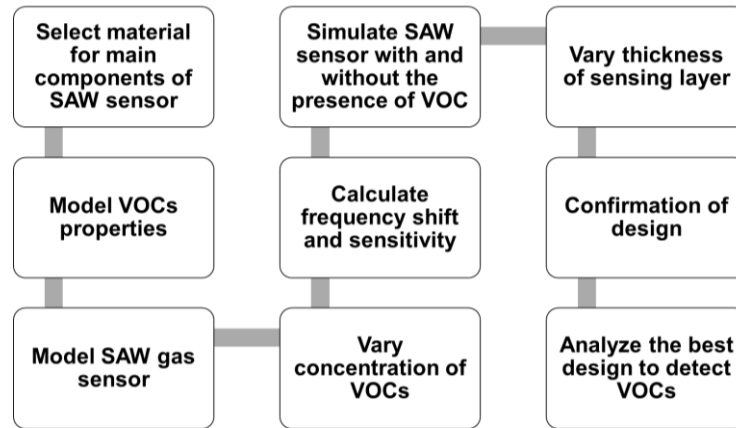   v.   mass of concentration of the VOCs in the polymers.

Fig. 2. The detailed step to model and simulate the SAW sensor with polymer as the sensing layer in COMSOL

Table 1: Some of the required parameters of VOC

Sensing Layer	VOCs	Molar mass (g/mol)	Air partition constant (K)
PEI	Acetone	58.08	1.15644
	Benzene	78.11	1.65549
	Toluene	92.14	2.06606
PIB	Acetone	58.08	1.20675
	Benzene	78.11	2.20792
	Toluene	92.14	2.75624

As the polymers were not listed in the library of materials in COMSOL Multiphysics software, the parameters of the polymers were filled in manually. The parameters needed for each polymer were Young's modulus, the Poisson's ratio, the density, and the polymer's relative permittivity, which are shown in Table 2.

Next, the SAW sensor was simulated without the presence of VOCs to obtain the resonance frequency. After that, the thickness of the polymers was varied along with the concentration of VOCs. In order to determine the best configurations to detect acetone, benzene and toluene, the frequency shift was calculated.

Table 2: Parameters of PEI and PIB to be configured in COMSOL

	PEI	**PIB**
Young's modulus (GPa)	3.04	10
Poisson's ratio	0.4008	0.48
Density (g/m^3)	1.27	0.918
Relative permittivity	3.3	2.2

Then, the proposed structure of the SAW sensor is shown in Table 3 and Fig. 3. From a single cigarette, approximately 50 ppm up to 550 ppm of acetone is produced, 10 ppm up to 60 ppm of benzene is generated and 5 ppm to 80 ppm of toluene is generated [9] which is the reason behind the VOCs concentration range.

Table 3: The design of the SAW Sensor

| Components	Description
Interdigital transducer	Material: Aluminum (Al)
Piezoelectric substrate	Material: YZ lithium niobate Acoustic wave velocity: 3960 m/s
Sensing element	1. **Polyethyleneimine (PEI)** The thickness of the sensing layer varied from 400 nm up to 600 nm. 2. **Polyisobutylene (PIB)** The thickness of the sensing layer varied from 200 nm up to 900 nm.
Volatile organic compounds concentration	1. **Acetone:** Concentration of acetone varied from 50 ppm up to 550 ppm. 2. **Benzene:** Concentration of benzene varied from 10 ppm up to 60 ppm. 3. **Toluene:** Concentration of toluene varied from 5 ppm up to 80 ppm.
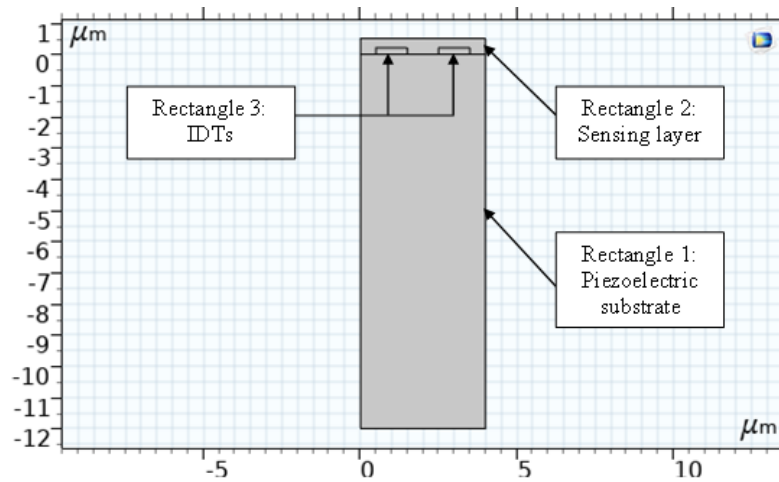
Fig. 3. Geometry of the SAW sensor that shows the interdigital transducer, the sensing layer and the piezoelectric substrate.

3. RESULT AND DATA ANALYSIS

3.1 SAW sensor with Polyethyleneimine (PEI) as the Sensing Layer

In order to study the effect of the thickness of sensing layers, the thickness of the PEI layer was varied between 400 nm, 500 nm, and 600 nm. Fig. 4, Fig. 5, and Fig. 6 show the changes in the frequency shift when this SAW configuration is used to detect acetone, benzene, and toluene respectively. As can be seen from all these figures, there is a significant change in the frequency shift between 400 nm and 500 nm thickness. In addition, since there is not much difference between 500 nm and 600 nm, it can be concluded that the optimum thickness of PEI to be used as the sensing layer with the SAW sensor is 500 nm.

3.2 SAW sensor with Polyisobutylene (PIB) as the Sensing Layer

Next, as for PIB, the thickness of the PIB layer varied from 200 nm to 900 nm. However, by referring to Fig. 7, the frequency shift increased steadily. Thus, the optimum thickness of the PIB layer could not be determined.

3.3 Effect of Concentration of VOCs towards frequency shift and sensitivity

In order to know the sensitivity of the sensing layers to each of the VOC, the approach is to set the thickness of the polymers to 500 nm and to choose the same concentrations for each VOC which is 50 ppm. Next, using Eq. (2) to calculate the sensitivity of the SAW sensor.

The sets of data for PEI and PIB are shown in Fig. 8 and Fig. 9 respectively.
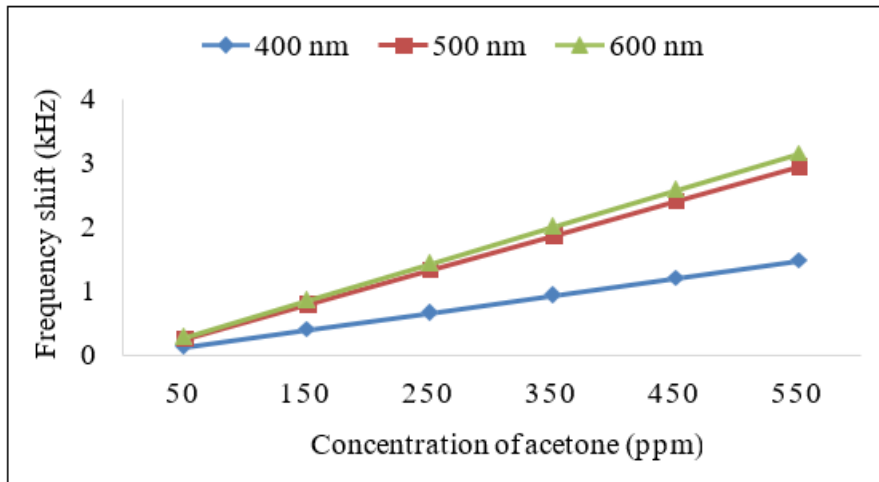
Fig. 4. SAW sensor with PEI sensing layer – detecting acetone
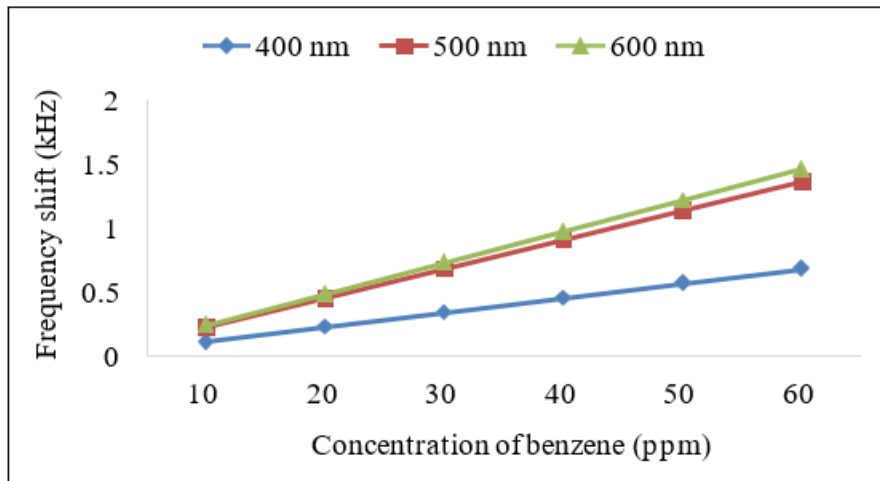
Fig. 5. SAW sensor with PEI sensing layer – detecting benzene
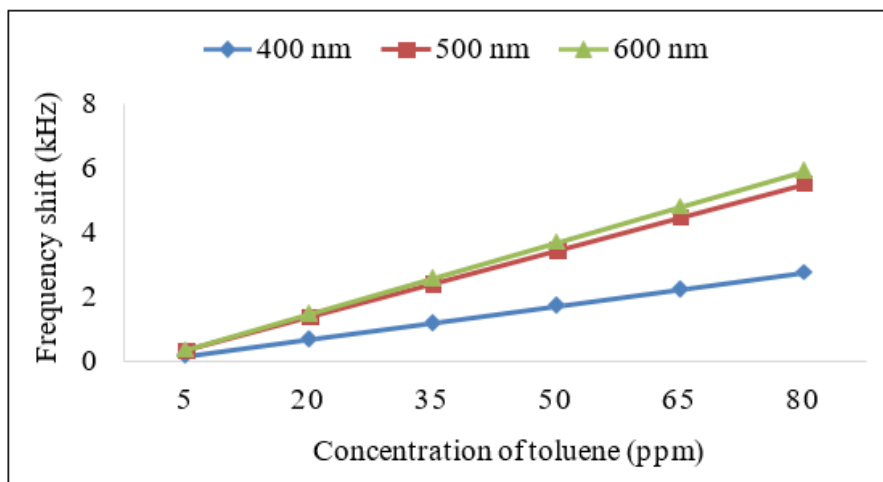
Fig. 6. SAW sensor with PEI sensing layer – detecting toluene
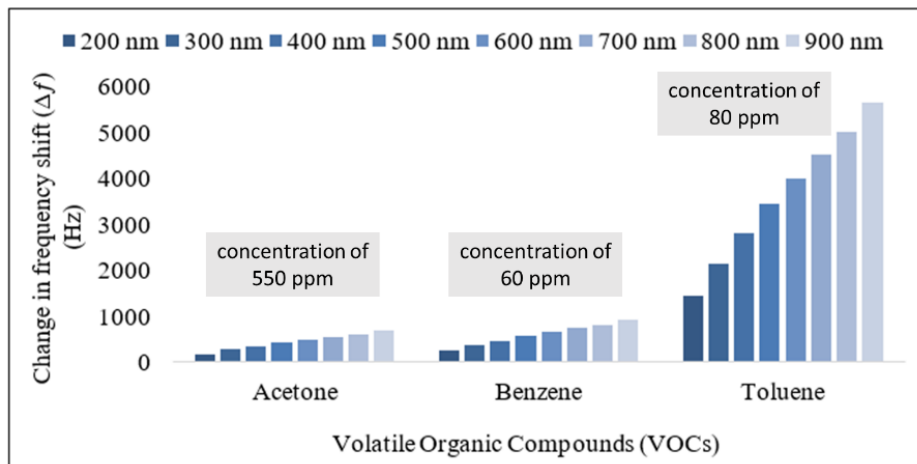
Fig. 7. Performance of PIB SAW sensor in sensing acetone, benzene, and toluene at specific concentrations.
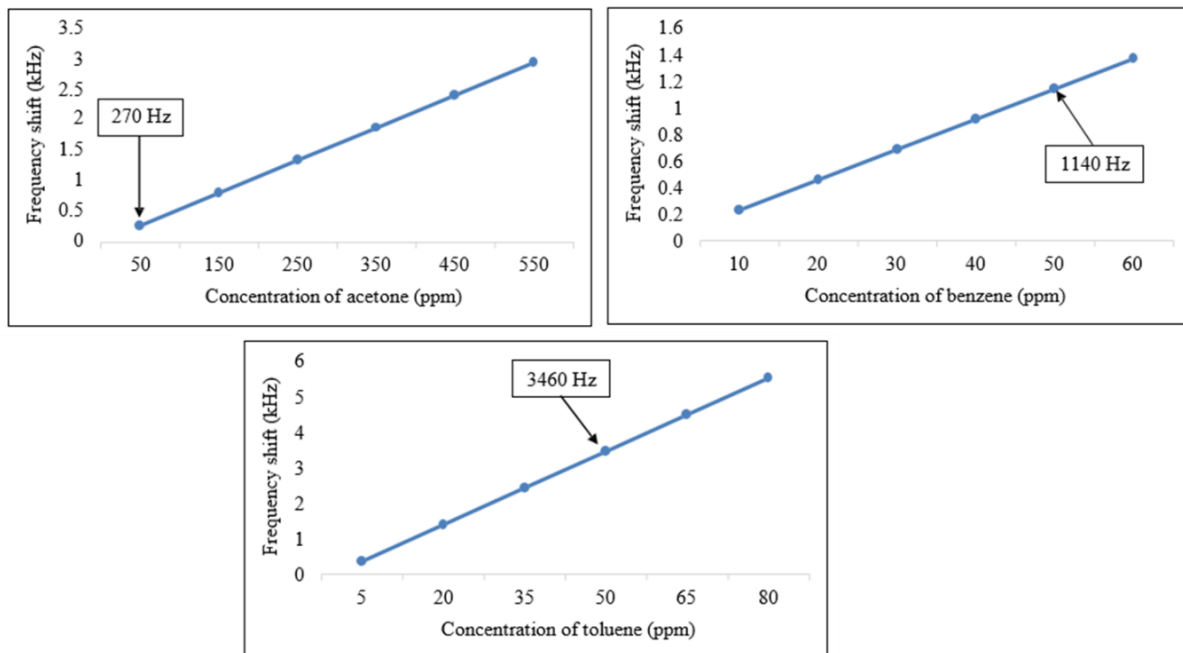
Fig. 8. The SAW sensor with PEI as the sensing element. The thickness of the PEI is set to 500 nm and the concentration of the VOCs is set to 50 ppm.

From these data, it can be concluded that PEI and PIB sensing layers are more sensitive towards toluene because the frequency shift caused by the presence of 50 ppm of toluene is the highest compared to acetone and benzene. Hence, it can also be assumed that both sensing layers will be more selective towards toluene when the three VOCs are presented on the surface of the sensor at the same time.

However, in comparison, for the detection of acetone and benzene, it can be observed that the PEI sensing layer is more suitable as it shows a much higher change in the frequency shift as compared to PIB.
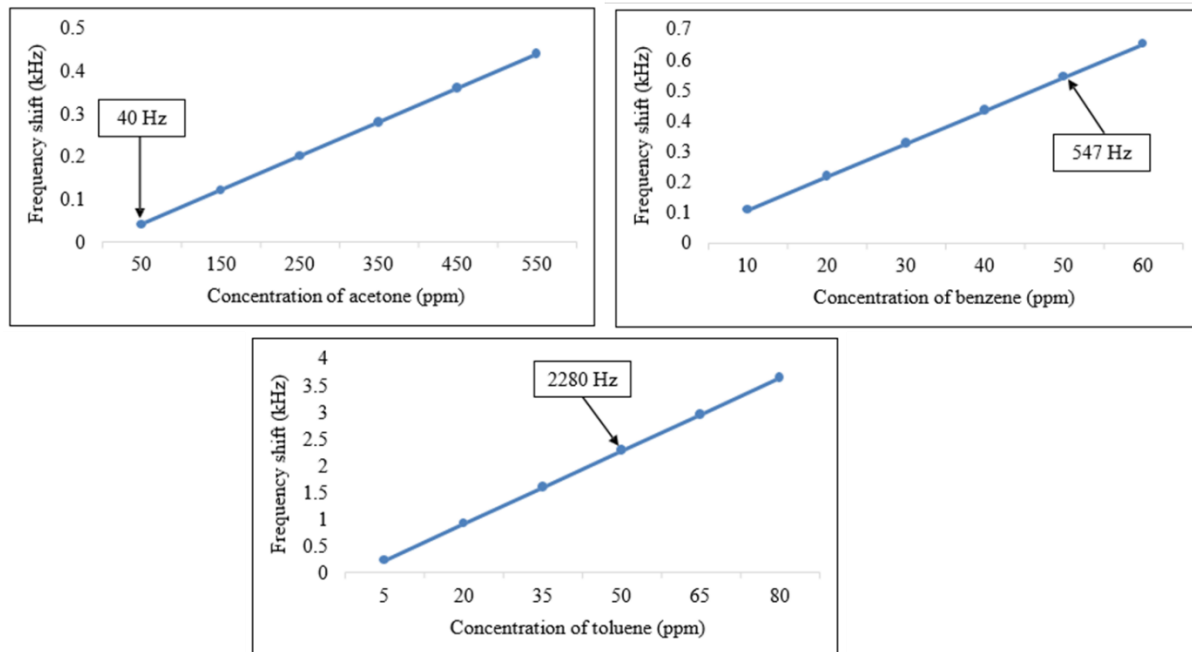
Fig. 9. The SAW sensor with PIB as the sensing element. The thickness of the PIB is set to 500 nm and the concentration of the VOCs is set to 50 ppm.

4. CONCLUSION

This work has presented a simulation of a polymer-based SAW sensor to detect acetone, benzene, and toluene. Two types of polymers were proposed as the sensing layers for the SAW sensor: polyethyleneimine (PEI) and polyisobutylene (PIB). Both configurations portrayed the same pattern where the frequency shift and sensitivity increase as the concentration of VOCs increases.

For PEI, the optimized thickness is 500 nm. Using the same thickness for PIB, the sensitivity of the sensors was investigated and both configurations produced promising results in sensing toluene even as low as 5 ppm. In detecting acetone and benzene, the PEI layer showed higher frequency shifts compared to the PIB layer.

REFERENCES

[1] C. Y. Cheng, S.-S. Huang, C.-M. Yang, K.-T. Tang and D.-J. Yao, "Detection of Cigarette Smoke Using a Surface-Acoustic-Wave Gas Sensor with Non-Polymer-Based Oxidized Hollow Mesoporous Carbon Nanospheres," pp. 1-11, 2019.

[2] B. Szulczynski and J. Gebicki, "Currently Commercially Available Chemical Sensors Employed for Detection of Volatile Organic Compounds in Outdoor and Indoor Air," pp. 1-15, 2017.

[3] G. Panneerselvam, V. Thirumal and H. M. Pandya, "Review of Surface Acoustic Wave Sensors for the Detection and Identification of Toxic Environmental Gases/Vapours," Archives of Acoustics, vol. 43, pp. 357--367, 2018.

[4] V. Ionescu, "Design and Analysis of a Rayleigh SAW Resonator for Gas Detecting Applications," Rom. Journ. Phys., vol. 60, pp. 502-511, 2015

[5] V. Lukose and H. B. Nemade, "Finite element simulation of one-port surface acoustic wave resonator with thick interdigital transducer for gas sensing," pp. 1-6, 2018.

[6] C. Tasaltin, M. A. Ali Ebeoglu and Z. Z. Ozturk, "Acoustoelectric Effect on the Responses of SAW Sensors Coated with Electrospun ZnO Nanostructured Thin Film," Sensors, no. 12, pp. 12006-12015, 2012.

[7] D. Matatagui, J. Marti, M. J. Fernandez, J. L. Fontecha, J. Gutierrez, I. Gracia, C. Cane and M. C. Horrillo, "Optimized design of a SAW sensor array for chemical warfare agents simulants detection," Procedia Chemistry 1, pp. 232-235, 2009.

[8]   M. N. Hamidon and Z. Yunusa, "Sensing Materials for Surface Acoustic Wave Chemical Sensors," in Progresses in Chemical Sensor, INTECH, pp. 161-179.

[9]   Centers for Disease Control and Prevention (US); National Center for Chronic Disease Prevention and Health Promotion (US); Office on Smoking and Health (US), "Chemistry and Toxicology of Cigarette Smoke and Biomarkers of Exposure and Harm," in How Tobacco Smoke Causes Disease: The Biology and Behavioural Basis for Smoking-Attributable Disease: A Report of the Surgeon General, Atlanta, Centers for Disease Control and Prevention (US), 2010.

Performance Prediction of DC Motor Fed From Half-Controlled Bridge Rectifier

Bilal A. Nasir[1*]

[1]*Dep. Electrical Technologies, Northern Technical University, Kirkuk, Iraq*

Corresponding author: Bilal Abdullah Nasir, bilalalnasir@ntu.edu.iq

Abstract— Controlled rectification is the process of obtaining a controlled output DC voltage from a constant AC voltage. This can be used in the speed control of the DC motor to provide rapid torque control and a quick starting response. In this work, a three-phase half-controlled bridge rectifier has been used. The average output DC voltage varies smoothly by varying the firing angle (α). Different methods of analysis such as state-space and Fourier-series, are used to obtain the performance of the DC motor fed from the bridge-rectifier supply. However, these methods do not deal with the prediction of the discontinuous conduction phenomenon which occurs during the operation of the DC motor with a variation of delay angle. This paper deals with the prediction of performance characteristics during the operation of the DC motor fed by a 3-phase half-controlled bridge rectifier, including the transient as well as steady-state operation with a variation of delay angle as well as application of load torque at starting.

1. INTRODUCTION

The 3-phase half-controlled rectifier is the most frequently used in DC motor control systems. Two of the six semiconductor devices, one thyristor and one diode conduct at any time instant, as shown in Figure 1. The gating of each thyristor initiates a pulse of load current. Therefore, this is a six-pulse half-controlled rectifier [1-10]. The Simulink model is shown in Figure 2.
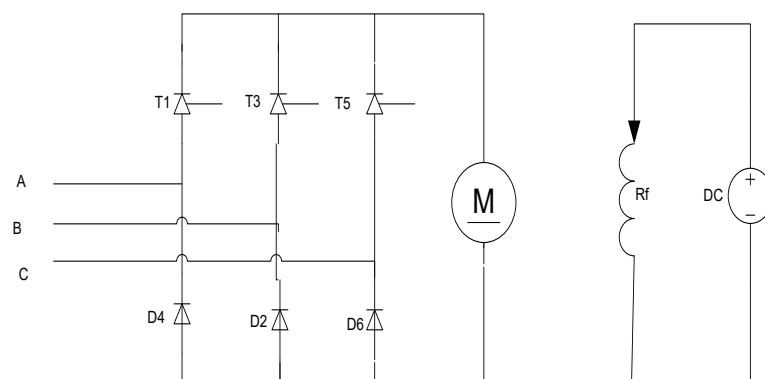
Fig. 1. Schematic diagram of the Circuit

Controlled rectification is the process of obtaining a controlled output DC voltage from a constant AC voltage. This can be used in the speed control of the DC motor to provide rapid torque control and a quick starting response [11-16]. In this work, a three-phase half-controlled bridge rectifier has been used. The average output DC voltage varies smoothly by varying the firing angle (α). Different methods of analysis such as state-space and Fourier-series are used to obtain the performance of the DC motor fed from the bridge-rectifier supply

[17-21]. But these methods do not deal with the prediction of the discontinuous conduction phenomenon which occurs during the operation of the DC motor with a variation of delay angle. This paper deals with the prediction of performance characteristics during the conduction operation of the DC motor fed by a 3-phase half-controlled bridge rectifier, including the transient and steady-state operation with a variation of delay angle as well as the application of load torque at starting. Up to our knowledge and from the literature survey, the reasons for the discontinuous operation of the DC motor fed from a controlled rectifier, as well as their effects on the motor performance, have not been studied in any published work. An analytical solution is used to study the parameters governing the discontinuous conduction phenomenon.
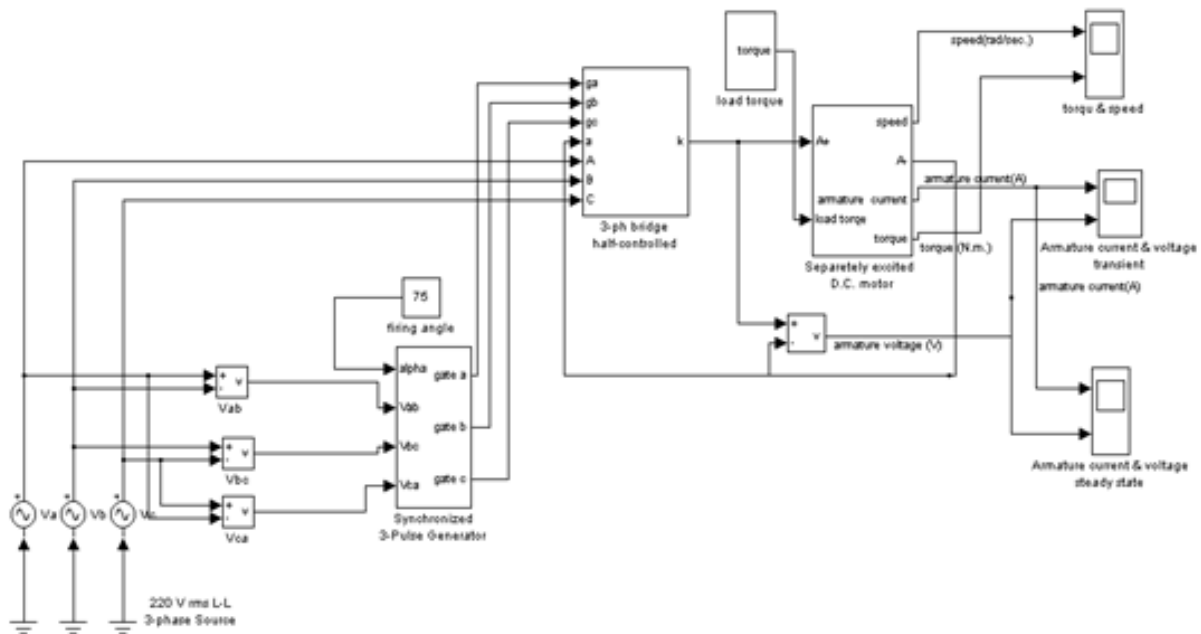
Fig. 2. Simulink Model for the 3-phase half-controlled rectifier.

2. SYSTEM ANALYSIS

2.1 Numerical Solution [2]

The DC motor fed from a half-controlled 3-phase bridge rectifier supply is shown in figure (1). The system is represented by the following voltage and torque balance linear differential equations:

$$\frac{di_a(t)}{dt} = \frac{1}{L_a}\left(V_a(t) - R_a \bullet i_a(t) - K_m \bullet w(t)\right) \tag{1}$$

$$\frac{dw(t)}{dt} = \frac{1}{J}\left(K_m \bullet i_a(t) - B \bullet w(t) - T_L\right) \tag{2}$$

Where:

V_a= average motor armature voltage (V).
i_a= instantaneous motor armature current (A).
$w(t)$= instantaneous motor speed (rad./sec.).
B= motor torque friction or damping coefficient (N.m/rad./sec.).
K_m= motor constant (N.m/A).
J= motor moment of inertia (Kg.m^2)
L_a= motor armature inductance. (H)
R_a= motor armature resistance. (Ω)

T_L= motor load torque (N.m)

There are two distinct cases in which the conduction periods of the

thyristors and diodes are different. These cases are α≤60° and α>60°, where (α) is the firing delay angle of the thyristors. Tables (1) and (2) give the conduction periods of thyristors and diodes and the armature voltage for α≤60° and α>60°, respectively.

Table 1: 3-phase bridge half-controlled rectifier (α≤60°).

Conduction period (degree)	Conduction Thyristor and Diode	Load voltage(Va)
$\alpha \rightarrow 60 + \alpha$ $60 + \alpha \rightarrow 120 + \alpha$ $120 + \alpha \rightarrow 180 + \alpha$ $180 + \alpha \rightarrow 240 + \alpha$ $240 + \alpha \rightarrow 300 + \alpha$ $300 + \alpha \rightarrow 360 + \alpha$	T_1 **&** D_6 T_1 **&** D_2 T_3 **&** D_2 T_3 **&** D_4 T_5 **&** D_4 T_5 **&** D_6	V_{ab} V_{ac} V_{bc} V_{ba} V_{ca} V_{cb}

Table 2: 3-phase bridge half-controlled rectifier (α≥60°).

Conduction period (degree)	Conduction Thyristor and Diode	Load voltage(Va)
$\alpha \rightarrow 60 + \alpha$ $60 + \alpha \rightarrow 120 + \alpha$ $120 + \alpha \rightarrow 180 + \alpha$ $180 + \alpha \rightarrow 240 + \alpha$ $240 + \alpha \rightarrow 300 + \alpha$ $300 + \alpha \rightarrow 360 + \alpha$	T_1 **&**D_6 T_1 **&** D_2 T_3 **&** D_2 T_3 **&** D_4 T_5 **&** D_4 T_5 **&** D_6	V_{ab} zero V_{bc} zero V_{ca} zero

Where

V_{ab}=$V_{Lm}sin(wt+60)$
V_{ac}=$V_{Lm}sin(wt)$
V_{bc}=$V_{Lm}sin(wt-60)$

The computation starts with initial conditions i_a=0 , w=0 and wt= α. Then, the computer calculates the new values of armature current and speed at each iteration step, and the rectifier is tested whether in the ON or OFF state of conduction. If the rectifier is in the OFF state, then the equation (1) above vanishes, and equation (2) becomes:

$$\frac{dw(t)}{dt} = \frac{1}{J}\left(-B \bullet w(t) - T_L\right) \tag{3}$$

If at any instant (i_a= 0) (discontinuous conduction state), equation (3) has to be solved for succeeding iterations until the rectifier becomes in ON state. A flow chart of the computer program is shown in Figure 3. Both transients, as well as steady-state solutions are obtained.
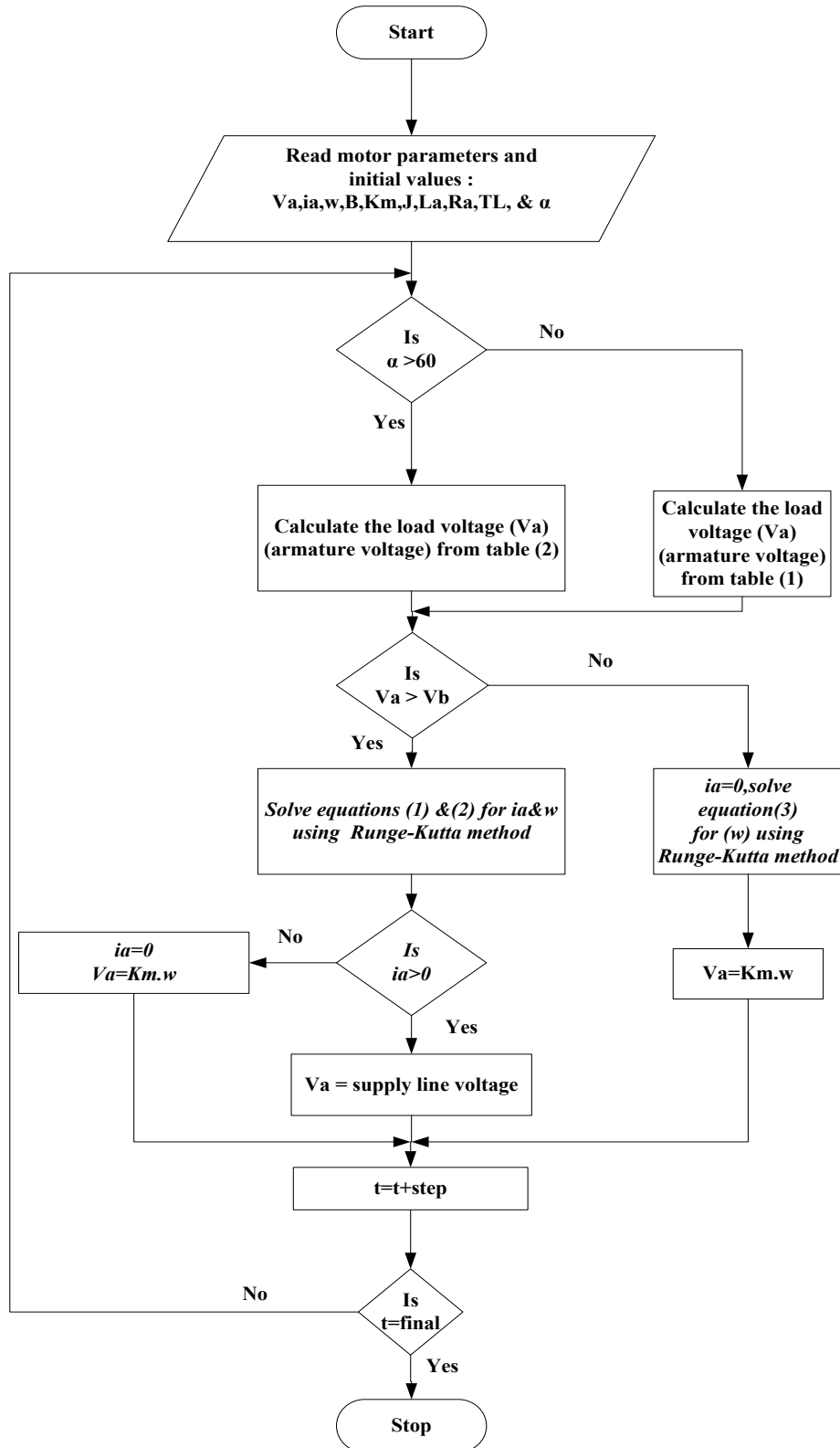

Fig. 3. Flowchart of the computer program.

2.2 Analytical solution [3]

During the ON state of the rectifier, the instantaneous armature current equation can be written as:

$$i_a(t) = \frac{V_{Lm}}{Z}\sin(wt + \alpha - \Phi) - \frac{V_b}{R_a} + \left\{\frac{V_b}{R_a} - \frac{V_{Lm}}{Z}\sin(\alpha - \Phi)\right\}e^{-\frac{R_a}{L_a}t} \tag{4}$$

Where V_{Lm}=maximum 3-phase supply line voltage.

$$Z = \sqrt{R_a^2 + X_{La}^2}$$ =armature impedance (Ω).

$$\Phi = \tan^{-1}\left(\frac{X_{La}}{R_a}\right)$$ =impedance angle.

V_b = armature back e.m.f = $K_m.w$(t)

In case of discontinuous conduction, the following condition must be satisfied in equation (4):

$(i_a(\text{t})) = \textbf{0 at } wt = \textbf{0}$ \hfill **(5)**

$(i_a(\text{t})) = \textbf{0 at } wt = \boldsymbol{\theta}$ \hfill **(6)**

Where (θ) is the conduction angle of the rectifier. In a discontinuous conduction: $\theta = (2\Pi/3) - \Delta$.

Where Δ is the discontinuous conduction angle. From equations(4-5), the condition of discontinuous conduction is derived as:

$$\frac{V_b}{R_a} \geq \frac{V_{Lm}}{Z}\sin(\alpha - \Phi) \tag{7}$$

Also, to find the discontinuous conduction angle (Δ), equation (6) is substituted in equation (4), and the result is a transcendental equation that the computer can solve to find the angle (Δ).

3. RESULTS AND DISCUSSION

A Simulink/MATLAB results were taken on a small separately excited DC motor, which has the following parameters: R_a=4Ω, L_a=0.086 H, K_m=1.46 N.m/A, J=0.017 K_g.m^2, V_a=220 V, field resistance (R_f)=370 Ω, field voltage (V_f) =220 V, rated speed =1500 r.p.m and the rated power=1.2 KW. The motor is fed from a half-controlled rectifier connected to a 3-phase supply, 220 V line voltage, and (50) Hz supply frequency, as shown in Figure 1.

Figure (4) shows the MATLAB results for the armature voltage and armature current at the firing delay angle (α=30°) of the rectifier with the motor starting at no load torque. Figure (5) shows the steady-state armature voltage and current when (α=60°) with no-load torque. Figure (6) shows the steady-state armature voltage and current when (α=60°) with a load torque of (5) N.m. applied to the motor at start. From these results, it can be shown that the armature voltage and current are continuous for small values of firing delay angles and high load torque application. At the same time, they have become discontinuous, and spikes appear at light loads and high firing delay angles of the rectifier.
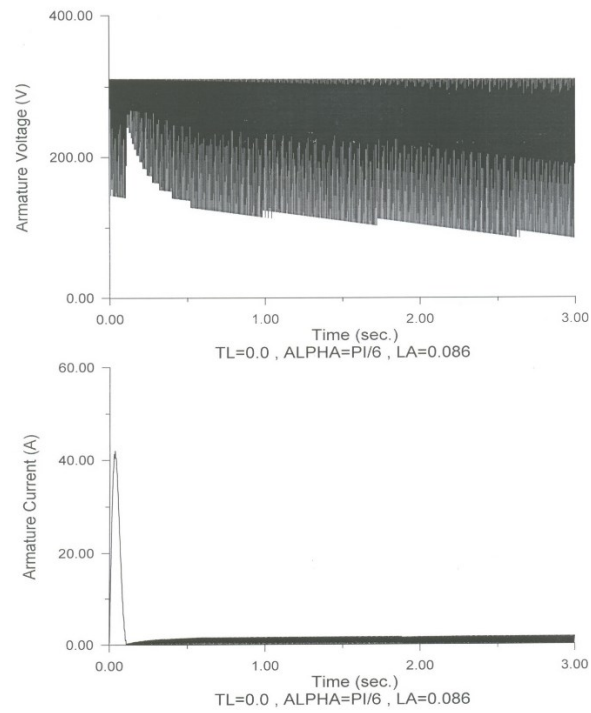
Fig. 4: Matlab results for starting of motor voltage and current.
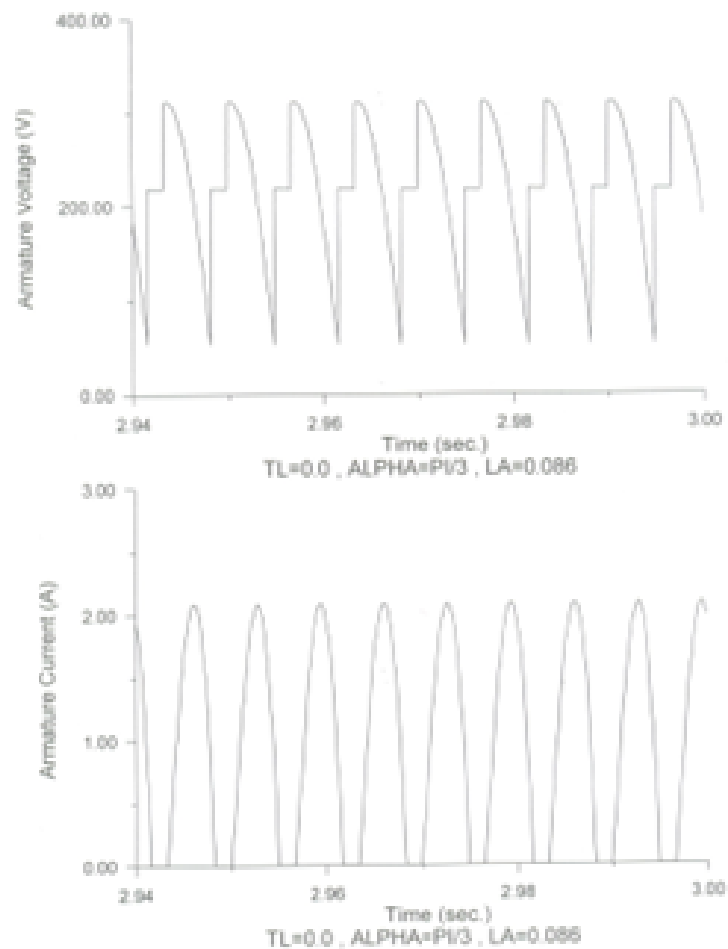
Fig. 5. Matlab results for steady-state motor voltage and current.
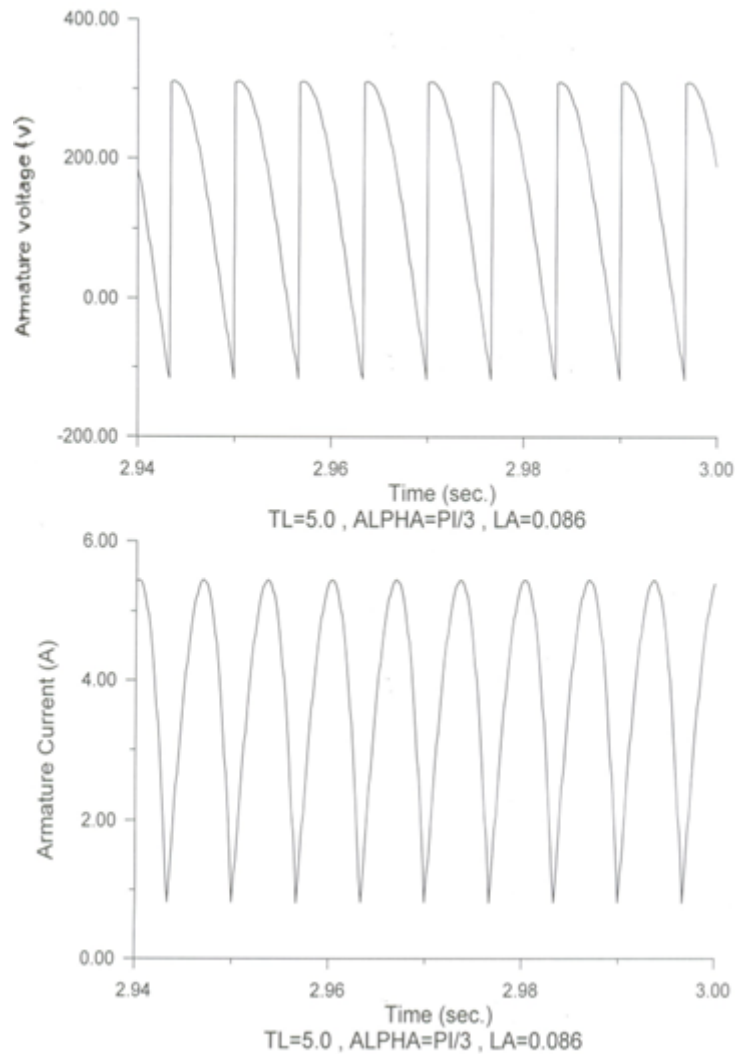
Fig. 6. Matlab results for steady-state motor voltage and current.

4. CONCLUSION

Numerical analysis using MATLAB/Simulink is applied for studying the performance of separately excited DC motor fed from a 3-phase bridge half–controlled rectifier. Motor voltage and current are obtained for both continuous and discontinuous conduction cases. It is noted that full load torque and advanced firing angles ($\alpha \leq 30^\circ$) lead to continuous conduction, while no-load torque and delayed firing angles ($\alpha \geq 30^\circ$) result in discontinuous conduction, and high spikes will appear in the motor voltage. From these results, the DC motor must be started at an advanced firing angle ($\alpha \leq 30^\circ$) with a load torque to avoid the discontinuous conduction case, which leads to a deterioration in the performance of the motor.

REFERENCES

[1]   M. Bogumila, " Modeling and Fuzzy Control of DC drives", 14th European Simulation Multi-Conference   ESMC2000,   Ghent,   PP186-190,   May   23-26,2000. https://www.academia.edu/1813510

[2]   PC Sen., " Principles of electric machines and power electronics", John Wily and Sons, New York, 2014. https://www.amazon.com/Principles-Electric-Machines-Electronics-Second/dp/0471022950

[3]   C. K.Venkateswarlu, and C. Chengaiah," Comparative study on dc motor speed control using various controllers", Journal of Research directions, volume 3, issue 1, pp6918-6925, Dec 2014. https://www.ijareeie.com/upload/2014/january/38_-COMPARATIVE.pdf

[4]   G.C.Ioannidis, C.S.Psomopoulos, S.D.Kaminaris, P.Pachos, H.Villiotis, S.Tsiolis, P.Malatestas, and G.A.Vokas, "AC-DC & DC-DC converters for dc motor drives", Proceedings of the International Conference on Electronics and Communication Systems, 2013. https://www.researchgate.net/publication/249993508

[5]   O. A. Alnathee," Performance of DC Motor Supplied From Single Phase AC-DC Rectifier", Power Electronics and Drives, Chapter Thirteen. https://www.philadelphia.edu.jo/academics/mlazim/page.php?id=13

[6]   R. Gupta, R. Lamba, and S. Padhee," Thyristor Based Speed Control Techniques of DC Motor: A Comparative Analysis ", International Journal of Scientific and Research Publications, Volume 2, Issue 6, pp1-6, June 2012. https://www.academia.edu/10629633

[7]   S. Shastri, and P. Pandey," A Comparative Analysis of Firing Angle Based Speed Control Scheme of DC Motor", International Journal of Engineering Research and Applications (IJERA), Vol. 3, Issue 4, pp.232-235, Jul.-Aug 2013. https://www.ijera.com/papers/Vol3_issue4/AM34232235.pdf.

[8]   D. Jaykishan, H. Moradiyal, and N. B. Danidhariya," Design and Simulation of Closed Loop Speed Control of DC Drive by Using Dual Converter", Volume 1, Issue 3, April 2014. DOI:10.21090/ijaerd.010330

[9]   R. Gupta and Ruchika," Thyristor Based DC Motor Control with Improved PF & THD", Vol. 5, No. 4, pp 519-536, December 2013. http://www.ijeei.org/docs-86020688652d3da2bbb032.pdf

[10]   H.F Soliman, and A.M Sharaf," An incremental fuzzy logic controller for separately excited dc motor-rectifier fed drive system", IEEE Canadian Conference of Electrical and Computer Engineering, Vol.1, 1994. DOI-10.1109/CCECE1994.405656

[11]   BK. Bose," Power electronics and motor drive recent technology advance ", Proceeding of IEEE International Symposium on Industrial Electronics, pp22-25, 2002. DOI: 10.1109/ISIE.2002.1026036

[12]   F. Song, Y. Zhang, Q. Tang, and L. Yaohua," Research on three-phase controlled rectifier bridge load simulation method", IEEE 11th Conference on Industrial Electronics and Application (ICIEA), 2016. DOI-10.1109/ICIEA.2016.7603709

[13]   R. G. Kanojiya, and P.M. Meshram," Optimal tuning of PI controller of speed control of dc motor drive using practical swarm optimization", APCET, 2012. DOI-10.11/APCET.2012.63032000

[14]   Y. A. Almatheel, and A. Abdelrahman, " speed control of dc motor using fuzzy logic controller", International Conference on Communication Control Computing and Electronic Engineering (ICCCCEE), 2017. DOI-10.1109/ICCCCEE.2017.7867673

[15]   C. Rajeswari, G.Sundradevi, A.Siva.Sankar, and C.Kokila, " Obtaining step response with small settling time using a fuzzy logic controller for separately excited dc motor" International Conference on Recent Advancement in electrical Electronic and Control Engineering, 2011. DOI-10.1109/ICONRAEeEC.2011.6129815.

[16]   M. Daigavane, H. Suryawanshi, and J. Khan, "A Novel Three-Phase Series-Parallel Resonant Converter Fed DCDrive System", Journal of Power Electronics, Vol. 7, No. 3, pp. 222-232, July 2007. https://www.koreascience.or.kr/article/JAKO200725522660230.page.

[17]   W. Phyo Aung, " Analysis on Modeling and Simulink of DC Motor and its Driving System Used for Wheeled Mobile Robot", World Academy of Science, Engineering and Technology 32, pp. 299-306, 2007. Corpus ID: 14196499.

[18] Gelen, and S. Ayasun, " Effects of PWM chopper drive on the torque-speed characteristic of DC motor", 43rd International Universities Power Engineering Conference, 2008. DOI: 10.1109/UPEC.2008.4651640

[19] C.S. Sharma, K. Singh, and R. Tamrakar," A Thyristor Based Speed Control Techniques Of Separately Excited Dc Motor", International Journal of Scientific Development and Research (IJSDR), Volume 1, Issue 11,pp13-25, November 2016. https://www.ijsdr.org/papers/IJSDR1611003.pdf.

[20] Tariq, M. F. Jalil, M. T. S. Beg, and M. A. Husain, "Simulation and Performance Analysis of a Thyristor Controlled d.c. Motor Drive", International Conference on Emerging Trends in Engineering and Technology, College Of Engineering, Teerthanker Mahaveer University, 2012. https://www.researchgate.net/profile/Mohammed-Husain-3/publication/280614000.

[21] Ellis, and Giritharan," Simulation and Analysis of Full Wave Bridge Rectifier Connected to DC/DC Buck Converter Feeding DC Motor", International Journal of Innovative Technology and Exploring Engineering (IJITEE), Volume-9, Issue-2, pp2993-2996, December 2019. https://www.ijitee.org/wp-content/uploads/papers/v9i2/B7750129219.pdf.

MATLAB-Based Vibration Signal Processing for Fault Diagnosis

S. M. A. Motakabber[1]*, Md. Mominul Hoque[1], Md. Rafiqul Islam[1], SI Ihsan[2],
GZ Islam[1] and AHM Zahirul Alam[1]

[1]Dept. of Electrical & Computer Engineering, International Islamic University Malaysia,
53100 Kuala Lumpur, Malaysia
[2]Dept. of Mechanical Engineering, International Islamic University Malaysia,
53100 Kuala Lumpur, Malaysia

*Corresponding author: amotakabber@iium.edu.my

Abstract— Traditionally, vibration signal processing has been performed using analog and digital signal analyzers or writing code in intermediate and high-level computer languages. However, the advent of higher-level interpretive-based signal processing software products such as MATLAB has added a new dimension to vibration signal processing. This paper presents a method for analyzing motor vibration data using MATLAB. The method first pre-processes the vibration data to remove noise and baseline wander. Then, the frequency spectrum of the vibration signal is calculated using the Fourier transform. The frequency spectrum is then used to identify the dominant frequencies in the vibration signal. These dominant frequencies can be used to identify potential problems with the motor, such as bearing defects or misalignment. The method was studied on a set of vibration data collected from open source online data of a real motor. The results showed that the method was able to identify the dominant frequencies in the vibration signal accurately. The method was also able to identify the potential problems with the motor. This paper demonstrates the effectiveness of using MATLAB for analyzing motor vibration data. The method presented in this paper can be used to improve the reliability and efficiency of motor maintenance.

1. INTRODUCTION

Rotating machinery signal analysis is the process of extracting information about the condition of rotating machinery from vibration signals. This information can be used to identify and diagnose faults, such as bearing defects, gear tooth wear, and misalignment [1]. MATLAB is a powerful software package that can be used for rotating machinery signal analysis. MATLAB provides a wide range of signal processing functions, including Fourier transforms, time-frequency analysis, and statistical analysis. MATLAB also provides powerful visualization tools that can be used to display and interpret vibration signals. The following are some of the steps involved in rotating machinery signal analysis using MATLAB [2][3]:

The first step is to collect vibration data from the rotating machinery. Collecting vibration data is an important part of the maintenance and monitoring of rotating machinery. Vibration data is a valuable source of information about the condition of rotating machinery.

There are a few different ways to collect vibration data. Accelerometers are the most common type of sensor used to collect vibration data. They measure the acceleration of the machinery, which can be used to calculate the vibration velocity and displacement. Vibration probes are used to measure vibration at specific points on the machinery. They are typically used in conjunction with accelerometers to provide more detailed information about the vibration at different locations. Laser vibrometers are non-contact sensors that can be used to measure vibration at very high speeds [4]. They are often used to measure vibration in rotating machinery, where it is difficult to attach accelerometers.

The following are some of the factors to consider when collecting vibration data. The type of machinery will

determine the type of sensor that is needed. For example, accelerometers are typically used to collect vibration data from rotating machinery, while vibration probes are typically used to collect vibration data from bearings. The sensors should be placed at locations where they can accurately measure the vibration. For example, accelerometers should be placed on the bearings and other critical components of the machinery. The sampling rate is the number of times per second that the vibration data is collected. The sampling rate should be high enough to capture the highest frequency of vibration that is present. The duration of the measurement should be long enough to capture a representative sample of the vibration.

Once the vibration data has been collected, it can be analyzed using a variety of software tools. These tools can be used to identify and diagnose faults, monitor the condition of the machinery, and optimize its performance.

The vibration data may need to be pre-processed before it can be analyzed. This may involve filtering out noise, removing baseline offsets, and normalizing the data. Perform signal analysis. The next step is to perform signal analysis on the pre-processed data. This may involve using Fourier transforms, time-frequency analysis, or statistical analysis to extract features from the data.

A transformation technique should be applied that converts the vibration signal to a different domain, such as the frequency domain or the time-frequency domain, which make the analysis easy and efficient.

2. USES OF MATLAB FOR VIBRATION DATA ANALYSIS

2.1 Interpret The Results

The final step is to interpret the results of the signal analysis. This may involve identifying and diagnosing faults or monitoring the condition of the rotating machinery. MATLAB is a versatile and powerful tool that can be used for a wide range of rotating machinery signal analysis tasks. Its flexibility and interactivity make it a valuable tool for engineers and technicians who need to quickly and easily analyze vibration signals. Here are some specific examples of how MATLAB can be used for rotating machinery signal analysis [5]:

2.2 Fault Detection

MATLAB can be used to identify and diagnose faults in rotating machinery by analyzing vibration signals. For example, MATLAB can be used to identify bearing defects by looking for changes in the frequency spectrum of the vibration signal. MATLAB can be used to monitor the condition of rotating machinery by tracking changes in vibration signals over time. This can be used to identify potential problems before they cause a failure.

2.3 Machine Optimization

MATLAB can be used to optimize the performance of rotating machinery by analyzing vibration signals. For example, MATLAB can be used to identify ways to reduce vibration levels or improve the efficiency of the machine. MATLAB is a valuable tool for engineers and technicians who need to analyze vibration signals from rotating machinery. Its flexibility, interactivity, and range of features make it a powerful tool for a variety of tasks, from fault detection to condition monitoring to machine optimization.

3. MATHEMATICAL MODELING

Mechanical vibration analysis often entails the use of intricate mathematical and statistical formulas. Fortunately, MATLAB tools greatly simplify the handling of such complexities. Assuming an electric motor is mounted on a spring-supported system, which includes a damper to reduce vibrations on the foundation, the following equations can be employed for the system's vibration analysis [6][7].

Equation of motion:

$$F(t) = m\ddot{x} + c\dot{x} + kx \qquad (1)$$

Where, $F(t)$ is the external force acting on the system m is the mass of the system, c is the damping coefficient of the system, k is the spring constant of the system and x is the displacement.

The natural frequency of vibration:

$$\omega_n = \sqrt{k/m} \qquad (2)$$

where, ω_n is the natural frequency of vibration in rad/s.

Damping ratio:

$$\zeta = c/2\sqrt{km} \tag{3}$$

where, ζ is the damping ratio.

Forced vibration response:

$$x(t) = A\sin(\omega t + \theta) \tag{4}$$

where, $x(t)$ is the displacement of the system at time t, A is the amplitude of vibration, ω is the frequency of the forcing function, and θ is the phase angle between the displacement and the forcing function.

3.1 Time-Domain Analysis

Step response:

$$x(t) = x_0\left(1 - e^{-t/\tau}\right) \tag{5}$$

where, x_0 is the initial displacement of the system at $t = 0$, and τ is the time constant of the system.

Impulse response:

$$h(t) = H\,\delta(t) \tag{6}$$

where, $h(t)$ is the impulse response of the system, H is the system gain, and $\delta(t)$ is the Dirac delta function.

Fourier transform:

$$X(\omega) = \int_{-\infty}^{\infty} x(t)\,e^{-j\omega t}dt \tag{7}$$

where, $X(\omega)$ is the Fourier transform of $x(t)$, and ω is the frequency variable.

3.2 Frequency-domain analysis

Frequency response:

$$H(\omega) = X(\omega)/X_0(\omega) \tag{8}$$

where, $H(\omega)$ is the frequency response of the system, $X(\omega)$ is the Fourier transform of $x(t)$ and $X_0(\omega)$ is the Fourier transform of $x_0(t)$.

Power spectral density (PSD):

$$S_x\,x(\omega) = |X(\omega)|^2 \tag{9}$$

where, $S_x\,x(\omega)$ is the PSD of $x(t)$, $|X(\omega)|$ is the magnitude of the Fourier transform of $x(t)$.

Cross-spectral density (CSD):

$$S_x\,y(\omega) = X(\omega)\,X^*(\omega) \tag{10}$$

where, $S_x\,y(\omega)$ is the CSD of $x(t)$ and $y(t)$, $X(\omega)$ is the Fourier transform of $x(t)$, and $X^*(\omega)$ is the complex conjugate of the Fourier transform of $x(t)$.

Wiener spectrum:

$$S_x\,x(\omega) = S_x\,x^*(\omega)|H(\omega)|^2 \tag{11}$$

where, $S_x\,x^*(\omega)$ is the power spectral density of the excitation, $|H(\omega)|$ is the magnitude of the frequency response.

4. RESULT AND DISCUSSION

The graphical representation of the time-domain and frequency-domain signals from a normally balanced rotating electric motor is displayed in Fig. 1(a) and (b), respectively. This graphical analysis was generated using MATLAB software. The data was captured from the sensor over a 10 ms time frame with a sampling rate of 20 kHz. In Fig. 1(b), although the motor was in a balanced condition, there are some spikes at the natural frequency and their harmonics, which is considered normal.
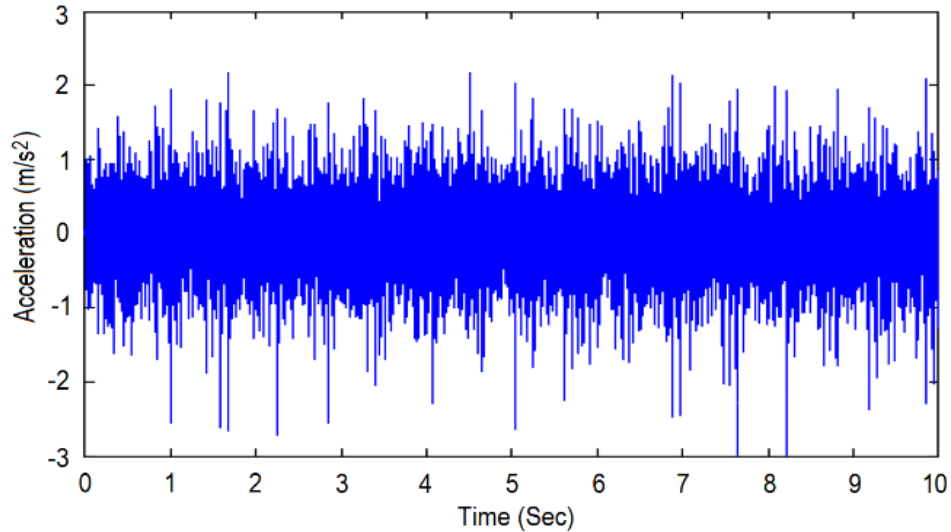
(a)
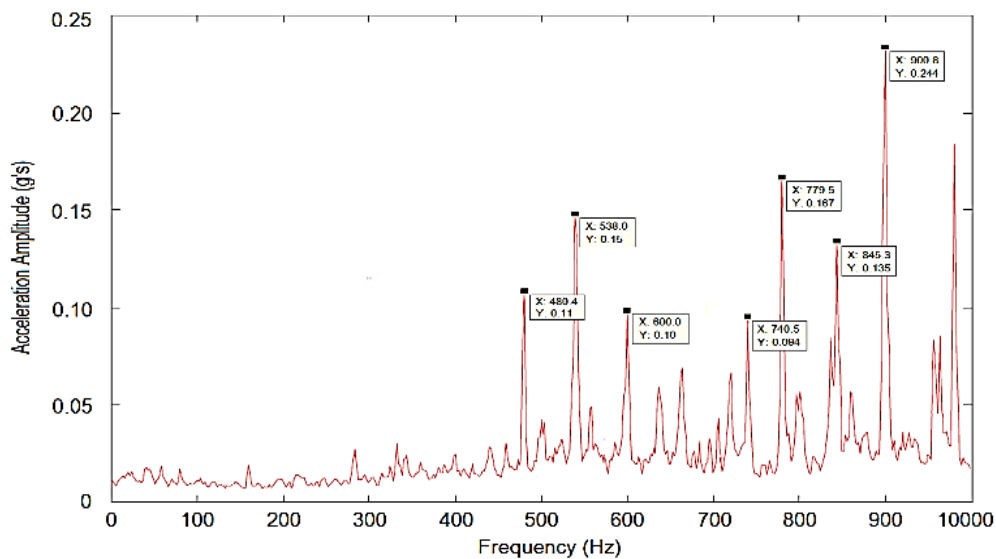
(b)

Fig. 1 Normal vibration signal of an electric motor, (a) time-domain and (b) frequency-domain

In contrast, the graphical representation of the time-domain and frequency-domain signals from the rotating electric motor in an imbalanced condition is shown in Fig. 2(a) and (b), respectively. It can be challenging to discern differences between the time-domain signals in Fig. 1(a) and Fig. 2(a) as they appear quite similar. However, the frequency-domain signals in Fig. 2(b) reveal new frequency spikes, and there is a higher frequency power distribution in the 700 Hz to 800 Hz frequency band compared to the frequency-domain signals in Fig. 1(b). These findings clearly indicate an abnormality or imbalance condition in the motor in the case of 2 (Fig. 2).

(a)

(b)
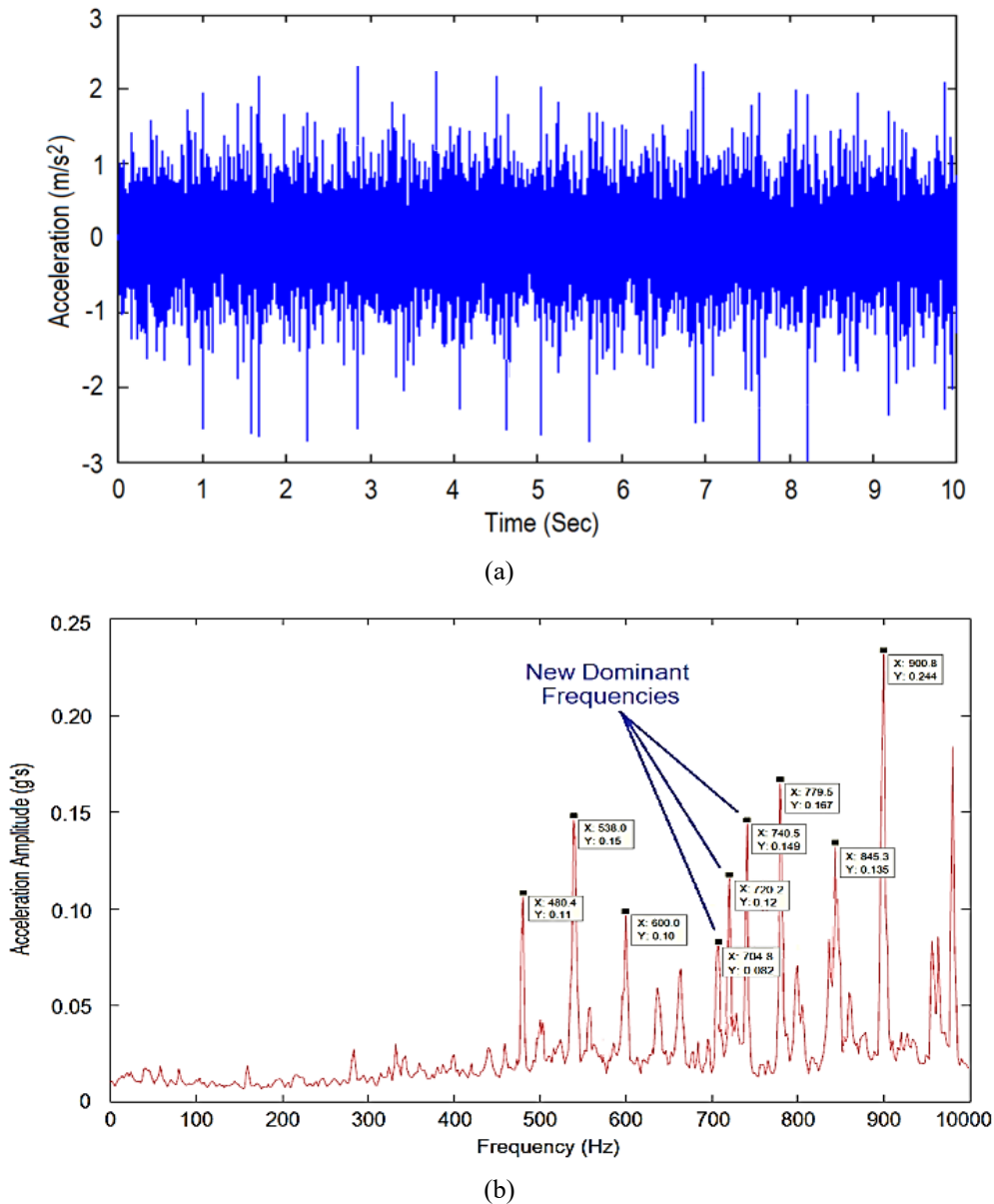
Fig. 2 Vibration signal of an imbalanced electric motor, (a) time-domain and (b) frequency-domain

5. CONCLUSION

Analyzing vibration data for electric motor balancing and health condition analysis can be a complex task. Nevertheless, MATLAB software tools can significantly simplify this analysis process. In this research, online real-time data from electric motors is employed to assess their condition. It's important to note that the accuracy of vibration data values depends on the sensor's placement [1]. However, the frequency spectrum trends in the data remain consistent for both healthy and faulty motors.

REFERENCES

[1] W. Zhu, H. Lin, W. Sun and J. Wei, "Vibration Performance of Traction Gearbox of a High-Speed Train: Theoretical Analysis and Experiments," Actuators, vol. 12(103), pp. 1-34, 2023.
[2] M. B. Joshi and K. S. Pujari, "Fault Diagnosis of High-Speed Rotating Machines Using MATLAB," Diagnostyka, vol. 24(2), pp. 1-8, 2023.

[3] S. Cho, K. Jeon and C. W. Kim, "Vibration Analysis of Electric Motors Considering Rotating Rotor Structure Using Flexible Multibody Dynamics-Electromagnetic-Structural Vibration Coupled Analysis," Journal of Computational Design and Engineering, vol. 10, pp. 578–588, 2023.

[4] Kang, S. G., La, J. P., Yoon, H. S., Choi, D. Y., & Park, K. H. "New Synthetic Heterodyne Laser Doppler Vibrometer for Measurement of Mechanical Vibrations with Submicron Amplitude," Key Engineering Materials, vol. 381–382, pp. 43–46, 2008.

[5] I. Howard, "Vibration Signal Processing Using MATLAB," Acoustics Australia, vol. 23(1), pp. 9-13, 1995.

[6] V. K. Ingle, and J. G. Proakis, Digital Signal Processing Using MATLAB, 3rd Ed. 3, Cengage Learning, 2011.

[7] S. Graham Kelly, Advanced Vibration Analysis, CRC Press, Taylor & Francis Group, New York, 2006.

Design and Performance Analysis of 28 GHz two-port MIMO Rectangular Microstrip Patch Antenna Array for 5G Applications

Shafiul Ismam[1], Delwar Hossain[2], and Syed Munimus Salam[*2]
Muhammad Mahbubur Rashid[3]

[1,2]*Dept. of EEE, Southern University, Chattagram, Bangladesh*
[*2]*Dept. of EEE, USTC, Chattagram, Bangladesh*
[3]*Department of Mechatronics, Faculty of Engineering, International Islamic University Malaysia*

Corresponding author: munim53@gmail.com

Abstract— A rectangular microstrip patch antenna array with two ports, designed for operation in the mm-wave band at 28 GHz for 5G applications, has been developed to exhibit superior gain and efficiency. This paper introduces a 12-element array activated by a feed network utilizing a T-junction power combiner/divider. The array elements consist of rectangular patch antennas inserted throughout the structure. The designed array antenna exhibited a measured impedance bandwidth of 1.42 GHz. The simulated findings indicate that the antenna achieved a favorable impedance match, with isolation levels below -22 dB throughout the frequency range. The whole substrate board dimensions were 19.99 × 26.968 × 0.254 mm3. The array is positioned on the substrate material known as Rogers RT5880, resulting in a consistent and reliable radiation pattern. The CST MWS software is employed to model and simulate the microstrip patch array antenna. CST MWS is an electromagnetic simulator utilizing the Finite Integration in Technique (FIT) methodology to model and analyze full-wave electromagnetic phenomena accurately. The realized gain of 15 dBi has been reached for the combined array, whereas the individual arrays have a realized gain of 12.3 dBi. The calculated overall efficiency is roughly -0.5 decibels. The antenna array under consideration has demonstrated favorable multiple-input multiple-output (MIMO) capabilities, as evidenced by an envelope correlation coefficient (ECC) of less than 0.1.

Keywords: *MIMO, 5G, and Antenna.*

1. INTRODUCTION

Antennas are fundamental components inside electric systems, establishing vital connections between transmitters and free space or between free space and receivers. Antennas play a crucial function in determining the properties of the system or device in which they are utilized. Antennas are utilized in various systems in diverse configurations. In specific systems, the operating parameters are intentionally aligned with the antennas' directional qualities or other relevant factors [1].

The ongoing progress in multimedia technology and the increasing demand for high-quality content and services have led to advancements in mobile communication, resulting in higher data capacity and faster speeds. As the rate at which data is transmitted and the number of mobile devices in use both experience exponential growth, the availability of frequency spectrum resources is becoming increasingly limited [2]. The forthcoming generation of cellular technology is poised to incorporate millimeter-wave (mm-Wave) bands, building upon the background. Due to the significantly wider bandwidth available in the mm-wave frequency spectrum compared to fourth generation/Long Term Evolution (4G/LTE) service, there is potential for substantial enhancements in data rate and capacity through a broader spectrum allocation.

The nascent technology necessitates antennas on user terminals that possess novel characteristics, including the ability to do spatial scanning through beamforming capabilities in their radiation patterns. This particular requirement presents a multitude of design challenges to strike a satisfactory balance between technological design considerations and commercial criteria. These criteria include cost-effectiveness, compact size, radiation efficiency, antenna gain, and broadband performance. Among the available options, microstrip antennas with coplanar arrangement of radiation elements and feeding network appear to be a favorable choice for achieving a functional component that offers a suitable combination of performance and manufacturing complexity, particularly for mobile applications [3].

The utilization of millimeter-wave (mmWave) carrier frequencies in forthcoming cellular networks and the implementation of high-gain adaptive antennas has been driven by the increasing need for high-speed cellular communications and the requirement for additional spectrum. The utilization of millimeter-wave channels has garnered significant interest due to their substantial bandwidth allocation. The user did not provide any text to rewrite.

The requirements of forthcoming mobile access technologies can be met by utilizing 5G mobile platforms. The U.S. Federal Communication Commission has undertaken an initiative to approve the utilization of licensed bands at frequencies of 28, 37, and 39 GHz as potential options for implementing 5G networks [5]. Designing antennas for frequencies of this magnitude presents various obstacles, yet it also has the advantage of occupying less physical area. As evidenced by empirical observations, the predominant design choice for 5G antennas is array structures. These designs effectively address the need for increased gain and directivity, a requirement that cannot be achieved using a single element.

Nonetheless, the performance in terms of capacity remains consistent for both a single element and an array, as the array is processed through a singular port. The frequency channel is consistently occupied for a significant duration, yet the demand for high data rates remains unmet. The empirical evidence indicates that implementing 5G networks necessitates the utilization of broader bandwidth and Multiple-Input Multiple-Output (MIMO) technology. The recommendation made by the Federal Communications Commission (FCC) has initiated a subsequent research phase focused on the development of Multiple-Input Multiple-Output (MIMO) antennas tailored explicitly for the 5G cellular spectrum [6-9]. The frequency that is considered particularly favorable for 5G cellular communication is the 28 GHz band [10-14].

Additionally, an ongoing study for optimizing MIMO arrays specifically for this spectrum [15-19]. The dimensions of the antenna are contingent upon the specific operating frequency. The high-frequency antenna efficiently operates within a limited physical space and requires careful attention during development.

Microstrip patch array antennas are widely used as printed resonant antennas in narrowband microwave wireless communications. These antennas can be effectively simulated using various software tools such as CST and HFSS. The determining factors for the optimal solution mainly lie in the structure's geometric characteristics and the desired precision level. In the context of time-domain analysis, CST is considered the most optimal simulator for structures with simple geometries, such as circular or rectangular shapes. The Computational Electromagnetics (CEM) method known as CST employs the Finite Integration Technique (FIT), a reliable discretization scheme for Maxwell's equations in their integral formulation. The matrix equations that arise from the discretization of the fields can be employed to conduct numerical simulations with improved efficiency. Using a planar Microstrip patch antenna, which possesses a regular shape, suggests that CST is a suitable and more proficient simulator compared to alternative simulation tools.

2. MOTIVATION

The rapid progress in wireless communication system technology has resulted in a significant need to create novel antenna structures. The microstrip array antenna has a contemporary design within the wireless communication system, rendering it a captivating subject for research. This technology is prevalent within mobile communication, primarily aimed at augmenting the system's scope and dependability. The necessity to develop a beam antenna that is high-gain, compact, and directional arises from the heightened attenuation experienced by high frequencies.

In addition, a significant proportion of the microstrip antenna array exhibits considerable size. One of the primary constraints associated with the typical microstrip antenna array design pertains to maintaining a specific inter-element spacing to minimize mutual coupling effectively.

2.1 Illustrations of Performance parameter

A parametric investigation was undertaken to analyze the impact of various antenna parameters on impedance matching characteristics, hence facilitating an examination of the influence of these parameters on the impedance bandwidth. This work holds significance as it contributes to the comprehension of antenna features for individuals involved in antenna design. The study investigated the impact of altering the patch width (W) and the gap between the patch and the ground plane (hs) on impedance bandwidth. These parameters were the most influential factors in determining the system's susceptibility. Furthermore, an investigation was conducted to examine the impact of the inset feed gap, patch length, and width. In the simulations, all parameters except the parameter of interest were held constant.

The dimensions of the ground plane play a crucial role in the design of narrowband antennas with a finite ground plane, as they are highly sensitive characteristics. Numerous researchers have noticed a significant correlation between the impedance bandwidth and the presence of a ground plane.

2.1.1. Quality factor, Bandwidth, Gain, Efficiency

The antenna figure-of-merit encompasses the quality factor, bandwidth, and efficiency, all of which are interconnected. It is important to note that these parameters cannot be individually optimized as a whole. Hence, a trade-off between these factors is inevitable while striving for optimal antenna performance. Frequently, there exists an inclination to maximize one variable while concurrently diminishing the efficacy of the other.

The quality factor is a metric that quantifies the antenna losses, serving as a figure of merit. Commonly observed in various systems, there are several types of losses: radiation, conduction (also known as ohmic), dielectric, and surface wave losses. Hence, the cumulative impact of these losses significantly affects the overall quality factor Q1, which is commonly denoted as [21].

$$\frac{1}{Q_t} = \frac{1}{Q_{rad}} + \frac{1}{Q_c} + \frac{1}{Q_d} + \frac{1}{Q_{sw}} \qquad \ldots \qquad \ldots \qquad 2.1$$

Where,

Q_t = total quality factor

Q_{rad} = quality factor due to radiation (space wave) losses

Q_c = quality factor due to condition (ohmic) losses

Q_d = quality factor due to dielectric losses

Q_{sw} = quality factor due to surface waves

In the case of substrates with extremely low thickness, the losses attributed to surface waves are negligible and can be disregarded. Nevertheless, it is imperative to consider thicker substrates in the analysis. As mentioned earlier, the losses can be mitigated by utilizing cavities as described in references [14] and [15].

Approximate formulas represent the quality factors of different losses for thin substrates (where the thickness is much smaller than the wavelength) of arbitrary shapes, such as rectangular and circular shapes [21]. These concepts can be articulated as follows.

$$Q_c = h\sqrt{\pi f \mu \sigma} \qquad \ldots \qquad \ldots \qquad \ldots \qquad 2.2$$

$$Q_d = \frac{1}{\tan \delta} \qquad \ldots \qquad \ldots \qquad \ldots \qquad 2.3$$

$$Q_{rad} = \frac{2\omega\epsilon_r}{hG_{t/l}}K \qquad \dots \qquad \dots \qquad \dots \qquad 2.4$$

The symbol tan δ represents the loss tangent of the substrate material, whereas σ denotes the conductivity of the conductors connected to the patch and ground plane. Gt/l represents the overall conductance per unit length of the radiating aperture.

The bandwidth of an antenna refers to the frequency range in which the antenna's performance, with respect to a specific attribute, meets a predetermined criterion. The bandwidth refers to the frequency range surrounding a central frequency within which the antenna's characteristics, including input impedance, pattern, beamwidth, polarization, sidelobe level, gain, beam direction, radiation, and efficiency, remain within an acceptable range. This acceptable range is determined by the ratio of the upper frequency to the lower frequency of operation.

As an illustration, a bandwidth ratio of 10:1 signifies that the top frequency is tenfold higher than the lower frequency. In the context of narrowband antennas, the bandwidth is commonly denoted as a proportion of the frequency deviation relative to the central frequency inside the bandwidth. For instance, a bandwidth of 5% signifies that the permissible range of frequencies for operation deviates by 5% from the center frequency of the bandwidth.

The fractional bandwidth of the antenna is inversely proportional to the Q_t of the antenna, and it is defined by

$$\frac{\Delta f}{f_0} = \frac{1}{Q_t} \qquad \dots \qquad \dots. \qquad 2.5$$

However, this approach may have limited utility as it fails to consider the important aspect of impedance matching at the input terminals of the antenna. A more comprehensive characterization of the fractional bandwidth pertains to a range of frequencies in which the Voltage Standing Wave Ratio (VSWR) at the input terminals is equal to or below the specified maximum threshold, assuming that the VSWR is unity at the designated frequency. A modified version of equation (2.5) that incorporates the consideration of impedance matching has been proposed in reference [21].

$$\frac{\Delta f}{f_0} = \frac{VSWR - 1}{Q_t\sqrt{VSWR}} \qquad \dots \qquad 2.6$$

In general, it is proportional to the volume, which for a rectangular microstrip antenna at a constant resonant frequency can be expressed as

$$BW \sim volume = area.\,height = length.\,width.\,height$$

$$\sim \frac{1}{\sqrt{\epsilon_r}}\frac{1}{\sqrt{\epsilon_r}}\sqrt{\epsilon_r} = \frac{1}{\sqrt{\epsilon_r}} \qquad \dots \qquad \dots \qquad 2.7$$

Hence, the relationship between the bandwidth and the dielectric constant of the substrate can be described as an inverse proportionality; namely, the bandwidth is inversely proportional to the square root of the dielectric constant. Figure 8 illustrates a standard representation of the bandwidth variation for a microstrip antenna with respect to the normalized height of the substrate. The relationship between substrate height and bandwidth is observed since an increase in substrate height leads to an increase in bandwidth.

The antenna's gain and directional capabilities: The gain of an antenna in a certain direction is defined as the ratio between the intensity of radiation in that direction and the intensity that would be observed if the power received by the antenna were radiated uniformly in all directions. The radiation intensity associated with the power radiated in all directions equally is equivalent to the power received by the antenna divided by 4π.

$$Gain = 4\pi\frac{radiation\ intensity}{total\ input\ (accepted\,)power} = 4\pi\frac{U(\theta,\emptyset)}{Pin}(dimensionless) \qquad \dots \qquad 2.8$$

When the direction is not started, the power gain is usually taken in the direction of maximum radiation.
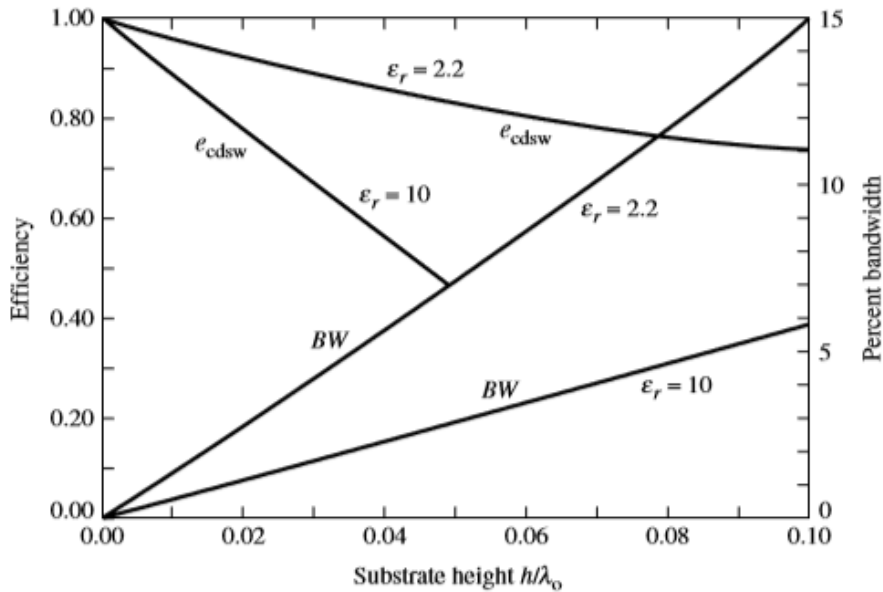
Figure 1: Efficiency and bandwidth versus substrate height at the resonant frequency for a rectangular microstrip

patch for two different substrates. SOURCE: [23].

The efficiency of antenna radiation can be determined by evaluating the ratio between the radiated power and the input power absorbed by the antenna. Computing an antenna's conduction and dielectric losses poses significant challenges, often necessitating testing techniques. Separating these losses is a complex task, as they tend to be intertwined and are commonly combined to determine the overall efficiency of the antenna, known as the effective conductivity and dielectric (ECD) efficiency. The resistance RL is employed to symbolize the losses associated with conduction and dielectric effects.
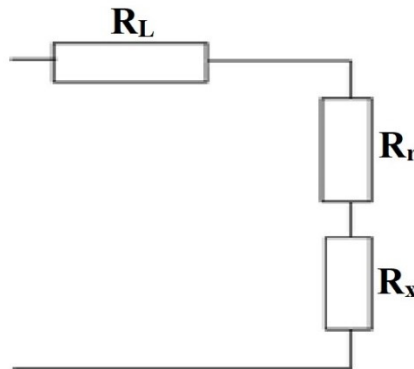
Figure 2: Conduction dielectric losses circuit.

The conduction-dielectric efficiency e_{cd} is defined as the ratio of the power delivered to the radiation resistance R_r to the power delivered to R_r and R_L, and the radiation efficiency can be written as

$$e_{cd} = \left[\frac{R_r}{R_L+R_r}\right] \qquad (dimensionless) \qquad \ldots \qquad 2.9$$

It is defined as the power radiated over the input power. It can also be expressed in terms of the quality factors, which for a microstrip antenna can be written as

$$e_{cdsw} = \left[\frac{1/Q_{rad}}{1/Q_t} = \frac{Q_t}{Q_{rad}} \right] \qquad \dots \qquad \dots \qquad 2.10$$

Where Q_t is given by 2.1, typically, variations of the efficiency as a function of the substrate height for a microstrip antenna with two different substrates are shown in Figure 8.

2.1.2. MIMO Antenna Overview

The concept of multiple input refers to a scenario in which multiple sources of input or the several-output (MIMO) technique involves the simultaneous use of several antennas at both the transmitter and receiver. This technique allows for the independent transmission of signals from the transmit antennas.

The utilization of numerous antennas enhances the transmission capacity within the constraints of restricted bandwidth and power levels. According to reference [22], in an optimal scenario, the channel capacity is directly correlated with the quantity of transmitter and reception antennas in a multipath environment.

$$C = B \log_2(1 + M \times N \times SNR) \qquad \dots \qquad \dots \qquad 2.11$$

where C is the channel capacity in bits/sec, B is the channel bandwidth in Hz, and M and N are the number of transmitter antennas and receiver antennas, respectively. SNR is the signal-to-noise ratio (absolute value). To be able to embed and integrate multiple antennas at the user terminal, size becomes a major limiting factor The need for compact MIMO antennas with good performance metrics is thus a major task.

In addition to the standard metrics and characteristics used to assess antenna performance, such as bandwidth, resonance frequency, radiation patterns, gain, and efficiency, it is crucial to examine a few significant factors in order to define a Multiple-Input Multiple-Output (MIMO) antenna system. As mentioned earlier, the metrics are not seen as important in single-antenna devices. However, they are considered crucial in the case of multi-antenna systems.

3. METHODOLOGY

The rationale for developing a finite array antenna is to create a compact, straightforward antenna that exhibits minimal aberrations while offering adequate bandwidth. Initially, a resonance-focused patch was developed to operate at a frequency of 28 GHz. Subsequently, a two-element array was constructed utilizing the corporate feed technique, which evenly distributes the incoming power into two separate paths. Subsequently, enhancements were made to the system's architecture and performance, resulting in the construction of a six-element array. This array features the alignment of two corporate feeds in series with the basic corporate feed. The incident power is distributed into three pathways at each junction during each occurrence. After successfully achieving satisfactory simulated performance of the one-port array, a twelve-element two-port array was then designed utilizing the identical structure. The performance of this multiple-input multiple-output (MIMO) system was then tested by simulation using CST software.

The finite array antenna is fabricated on a single surface of a Rogers RT5880 printed circuit board (PCB) substrate, which has a thickness of 0.254 mm. The PCB substrate possesses a relative permittivity of 2.2 and a loss tangent of 0.0009. The patch and the ground thickness are measured to be 0.035 mm. The material used for both components is copper in an annealed state. The corporate feed designs in CST utilized the analytical line impedance calculation functionality to determine and modify the width of the microstrip feedline. This adjustment was made to provide adequate impedance matching for feedlines with resistances of 50, 70, and 100 ohms.

The geometric parameters necessary to reach a resonance frequency of 28 GHz were computed and utilized in the design of a single patch. Subsequently, the patch's dimensions were further refined to attain the requisite resonance and performance characteristics. The configuration of the single patch is seen in Figure 13.

The optimized parameters of the single patch are listed in Table 2.1. The geometric parameters of the single patch structure can be adjusted to achieve the desired resonance.

Table-2.1 Dimension list of the Single patch antenna:

Dimension	Name	Value
Patch Width	W	3.46 mm
Patch Length	L	4.25 mm
Length of the Substrate	Lg	4.984 mm
Width of the Substrate	Wg	5.774 mm
Height of the substrate	hs	0.254 mm
Thickness of radiator	ht	0.035 mm
Length of feedline	Lf	1.73 mm
Length of inset	Fi	0.968 mm
The gap between the inset	Gpf	0.25 mm

Figure 3 illustrates the single patch antenna's 3D view and surface current.

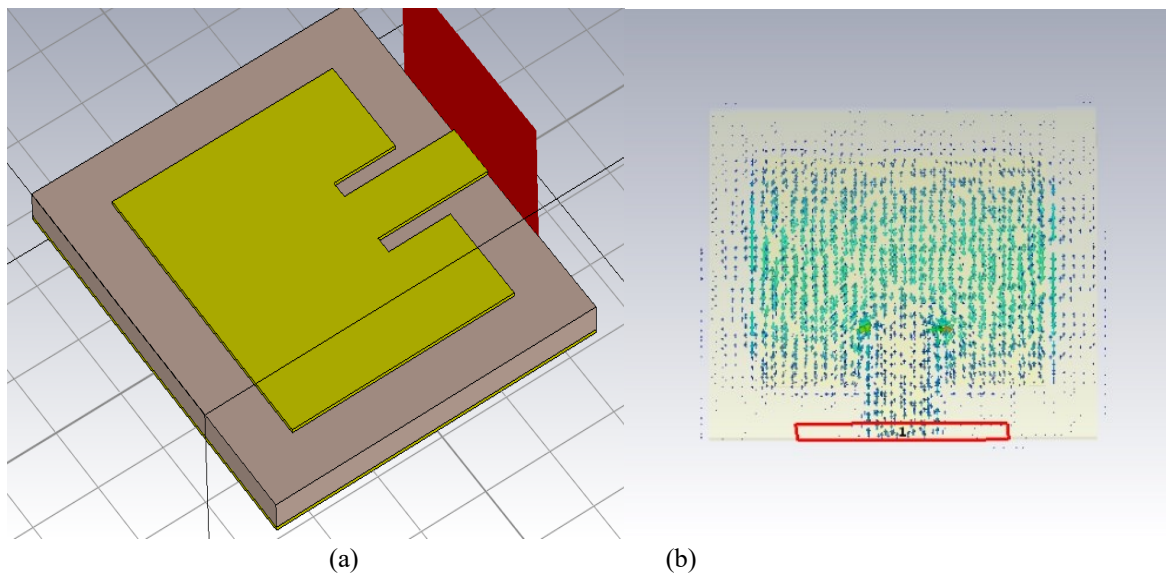

(a)   (b)
Figure 3: (a) 3D view and (b) Surface Current of the single patch antenna

The current distribution figure shows that the maximum area of the designed antenna is packed with current intensity and current density is at maximum right in the middle of the patch antenna, which is essential for efficient radiation.

The 6-element array is arranged side by side to establish a 12-element array powered by two waveguide ports to evaluate the array's MIMO performance. The spacing between a couple of arrays is 1.524 mm wide. In Figure 13, the 3D structure of the 12-element array is demonstrated.
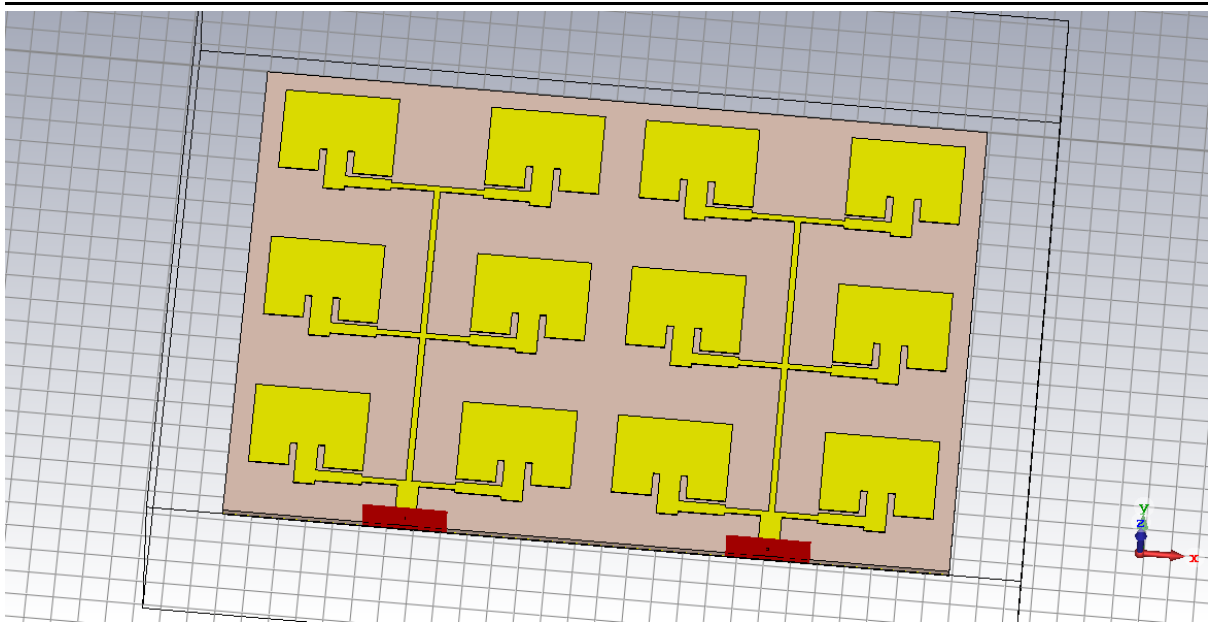
Figure 4: 3D structure of the 12-element 2-port array.

The overall dimensions for the substrate and ground of the one-port array and two-port array are categorized and listed in Table 2.2.

Table-2.2 Overall ground and substrate dimensions of the single array and the MIMO array:

Component	6 element array		12 element MIMO array	
	Length	Width	Length	Width
Substrate	19.99 mm	13.484 mm	19.99 mm	26.968 mm
Ground	19.99 mm	13.484 mm	19.99 mm	26.968 mm

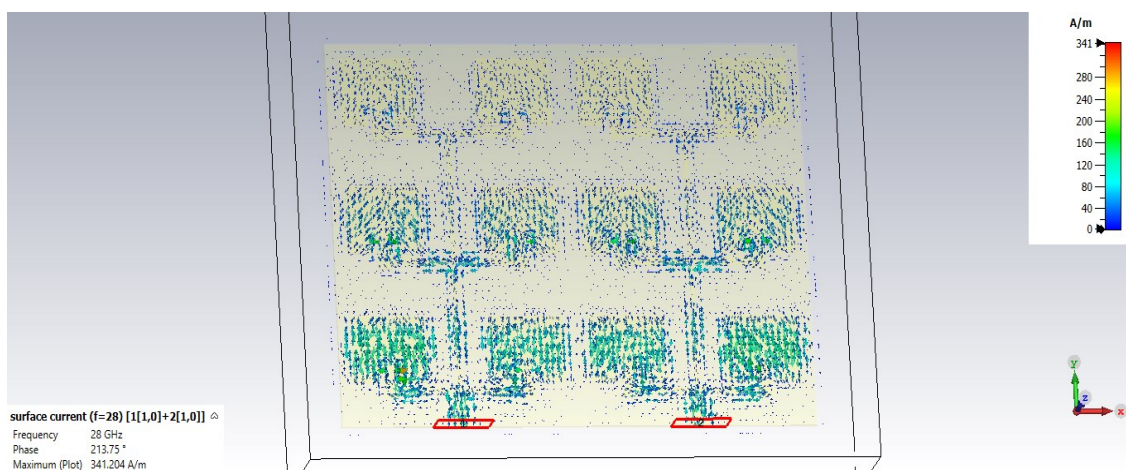The surface current of the 12-element array is portrayed in Figure 13.

Figure 5: Current distribution on the surface of the array antenna

As the figure shows, The current density and intensity of the array are relatively similar to the single port six-element array.

4. RESULT AND DISCUSSION

The performance of the proposed antenna array was evaluated and enhanced using the Finite Integration Technique within the CST microwave simulator. The parameters utilized in the analysis included dimensions obtained from equations and approximations (in the case of corporate feed). Subsequently, the parameters were optimized to improve the simulation results for return loss, VSWR, impedance characteristics, radiation pattern, and other relevant factors. This study evaluates simulated bandwidth, gain, efficiency, and MIMO performance of the corporate-fed two-port, 12-element array antenna. The assessment is conducted subsequent to the construction and design of the antenna.

VSWR parameter defines how well the antenna impedance matches the transmission line by taking the ratio of the reflected maximum and minimum voltage wave. A value of VSWR ≤ 2 is considered the primary requirement.
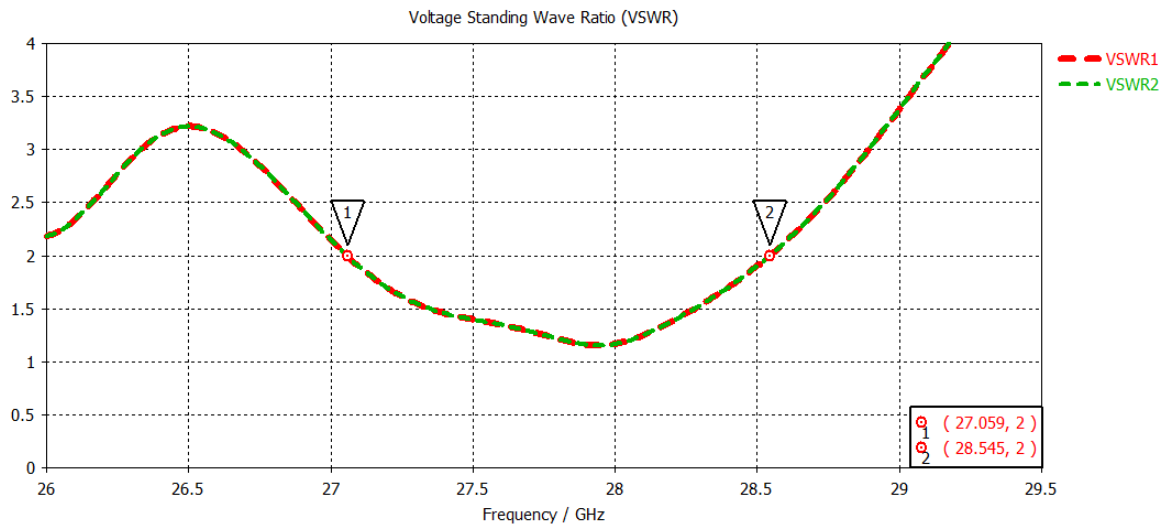
Figure 6: VSWR of the proposed array antenna

The plots of the VSWR of the proposed antenna in Fig. 16 show that the measured impedance bandwidth of the proposed antenna is 28 GHz for VSWR$\leq$2. Figure 7 demonstrates that the proposed antenna's reflection coefficients S11 and S22 are below -10dB, resonating in the mmWave frequency spectrum ranging from 27.09 to 28.51 GHz with a 1.42 GHz bandwidth.
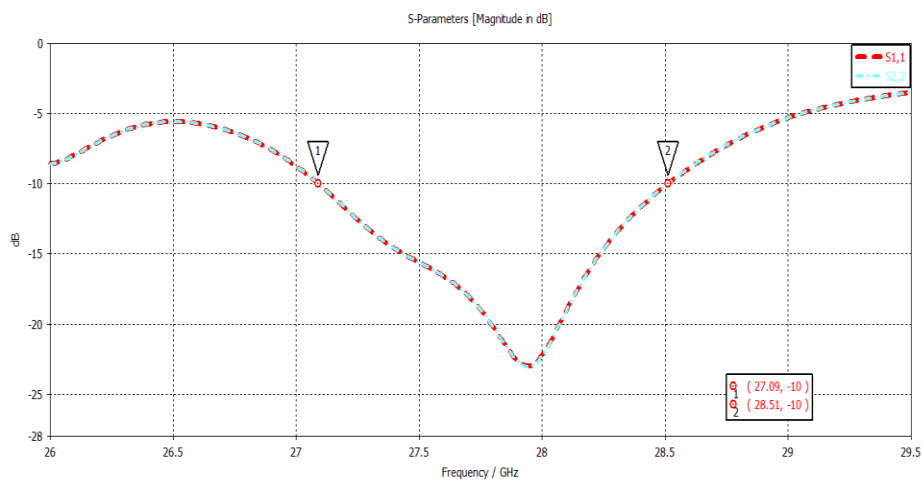
Figure 7: Reflection coefficient of the proposed array antenna

Figure 8 illustrates the transmission coefficients of the proposed antenna, which shows satisfactory isolation between the antenna ports. Where, $S_{12} = S_{21} < -20$ dB

Ismam et al.
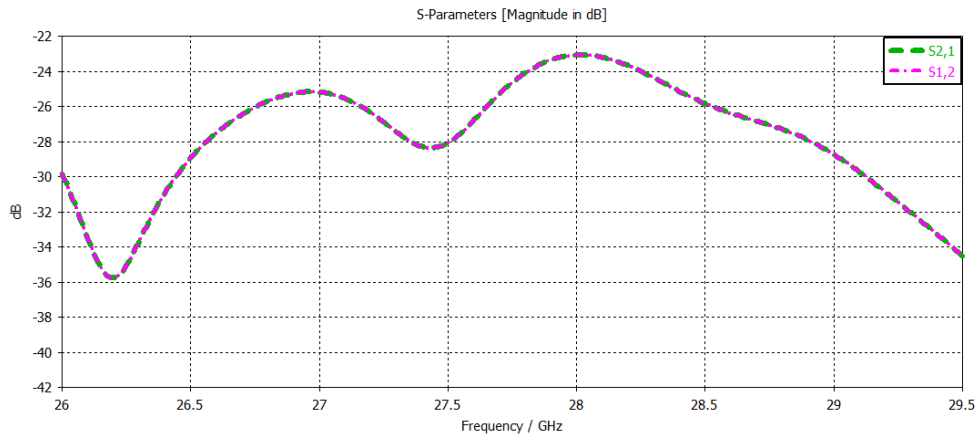
Figure 8: Transmission coefficient of the proposed array antenna

Radiation is the term used to represent the emission or reception of wave-front at the antenna, specifying its strength. Radiation Patterns are diagrammatical representations of the distribution of radiated energy into space as a function of direction.

(a)

(b)

Figure 9: 1D Far-field radiation pattern at 28GHz for (a) Phi=0^0, (b) Phi=90^0.

Figure 9 shows the 1D radiation pattern at 28 GHz with a main lobe magnitude of 12.8 dBi in realized gain with angular width of 19.3^0 for Phi=0^0(XZ plane) and main lobe magnitude of 15.1 dBi in realized gain with main lobe direction of 17^0 for Phi=90^0(YZ plane). Figure 21 shows the 3D radiation pattern of the proposed antenna in the XZ and YZ planes, illustrating that it is a directional antenna.
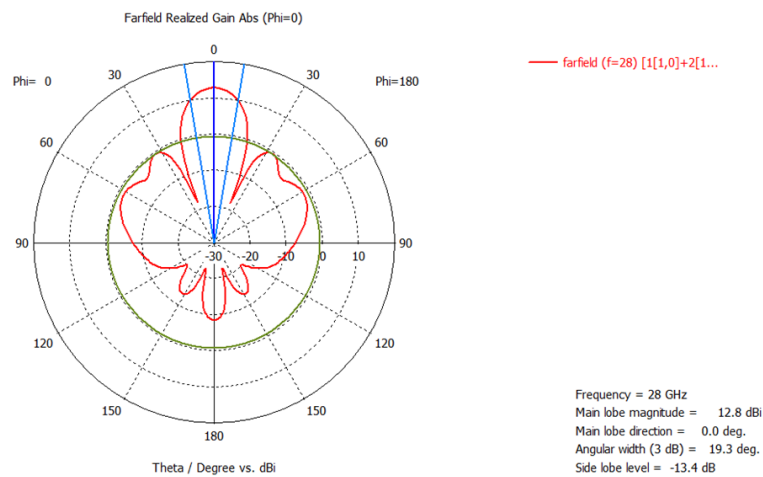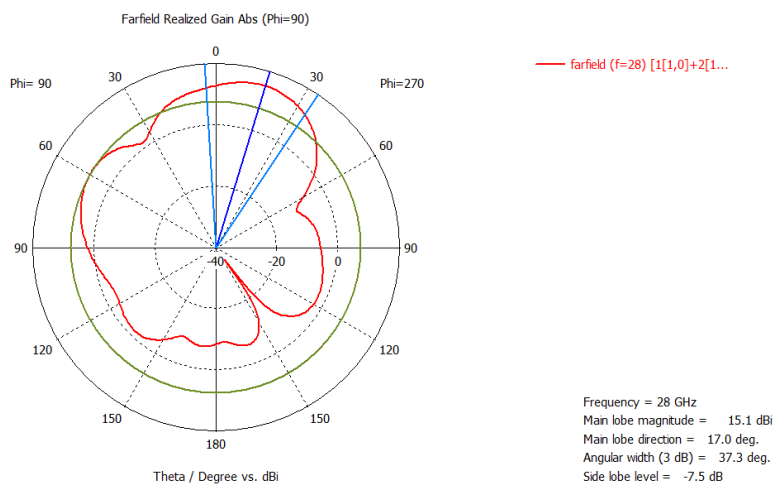
A comparison of the proposed antenna design with related works reported in the literature is listed in Table 4.1. The comparative analysis with other works shows that the proposed design demonstrates moderate compactness, bandwidth and gain performance. MIMO performance analysis is provided in detail for the proposed design, and it is observed that the MIMO antenna proposed in this work exhibits better performance as compared to other reported results. The suitability of the proposed MIMO array antenna for 28GHz mm–wave applications are established.

Table - 4.1 Performance comparison of this proposed antenna design with other recent works.

Reference	Frequency (GHz)	Board Size (mm^3)	No. of Ports	Bandwidth (GHz)	Gain (dBi)	ECC	Diversity Gain(dB)
[31]	3.6	$150 \times 75 \times 1.6$	8	1.2	2.5	<0.01	_
[32]	28	$41.3 \times 46 \times 0.5$	4	3.35	13.1	_	_
[33]	24	$15 \times 19 \times 0.254$	2	0.8	6	0.24	9.7
[34]	5.2 & 24	$40 \times 25 \times 0.254$	2	0.1 & 0.77	5 &7.3	_	_
[35]	28	$20 \times 20 \times 0.254$	2	0.85	8	0.13	9.9
This work	28	$19.99 \times 26.96 \times 0.254$	2	1.42	12.2	<0.01	10

5. CONCLUSION

The utilization of mmWave frequency bands is anticipated to address the current limited spectrum in wireless cellular networks. This study analyzes a planar patch antenna with a bandwidth of 1.42 GHz, which covers the 28 GHz 5G spectrum. The analysis includes a two-port 12-element MIMO configuration implemented on a Rogers RT Duroid 5880 substrate measuring $19.99 \times 26.96 \times 0.254$ mm3. The MIMO array antenna demonstrates a simple and compact structure, enabling operation within the frequency range of 27.09 GHz to 28.52 GHz. The measured peak gain for the proposed design is 12.3 dBi. Simulation results indicate a moderate impedance bandwidth with excellent matching and high isolation. Furthermore, the MIMO performance criteria, including a low ECC value, are satisfied. Consequently, the proposed architecture is suitable for future high-data-rate wireless networks.

REFERENCES

[1] Pramod Dhande, "Antennas and its Applications", Armament Research & Development Establishment, Dr. Homi Bhabha Rd, Pashan, Pune.
[2] W. F. Williams, "High-Efficiency Antenna Reflector", Microwave Journal, Vol. 8, July 1965.
[3] David Alvarez Outerelo, Ana Vazquez Alejos, Manuel Garcia Sanchez, Maria Vera Isasa, "Microstrip Antenna for 5G Broadband Communications: Overview of Design Issues", Department of Teoria de la Señal y Comunicaciones University of Vigo Vigo, Pontevedra, Spain.
[4] Y. Niu, Y. Li, D. Jin, L. Su, and A. V. Vasilakos, "A survey of millimeter wave communications (mmwave) for 5g: opportunities and challenges," Wireless Networks, vol. 21, no. 8, pp. 2657–2676, 2015.
[5] S. F. Jilani and A. Alomainy, "A Multiband Millimeter-Wave TwoDimensional Array Based on Enhanced Franklin Antenna for 5G Wireless Systems," IEEE Antennas and Wireless Propagation Letters, 2017.

[6]   X. Zhao, S. P. Yeo, and L. C. Ong, "Planar UWB MIMO Antenna With Pattern Diversity and Isolation Improvement for Mobile Platform Based on the Theory of Characteristic Modes," IEEE Transactions on Antennas and Propagation, vol. 66, no. 1, pp. 420–425, 2018.

[7]   N. Ashraf, O. M. Haraz, M. M. M. Ali, M. A. Ashraf, and S. A. S. Alshebili, "Optimized broadband and dual-band printed slot antennas for future millimeter wave mobile communication," AEU-International Journal of Electronics and Communications, vol. 70, no. 3, pp. 257–264, 2016.

[8]   Y. A. Hashem, O. M. Haraz, and E.-D. M. El-Sayed, "6-Element 28/38 GHz dual-band MIMO PIFA for future 5G cellular systems," in Antennas and Propagation (APSURSI), 2016 IEEE International Symposium on. IEEE, 2016, pp. 393–394

[9]   M. Ikram, M. Sharawi, K. Klionovski, and A. Shamim, "A switchedbeam millimeter-wave array with MIMO configuration for 5G applications," Microwave and Optical Technology Letters, vol. 60, no. 4, pp. 915–920, 2018.

[10]   D.M. Pozar, "Microstrip Antennas," Proc. IEEE, Vol. 80, No. 1, January 1992. © 1992 IEEE.

[11]   W. F. Richards, Y. T. Lo, and D. D. Harrison, "An Improved Theory of Microstrip Antennas with Applications", IEEE Trans. Antenna Propagat., Vol. AP-29, No. 1, January 1981.

[12]   C. M. Krowne, "Cylindrical-Rectangular Microstrip Antenna", IEEE Trans. Antenna Propagat., Vol. AP-31, No. 1, January 1983.

[13]   S. B. De Assis Fonseca and A. J. Giarola, "Microstrip Disk Antennas, Part 1: Efficiency of Space Wave Launching", IEEE Trans. Antenna Propagat., Vol. AP-29, No. 1, June 1984.

[14]   R. J. Mailloux, "On the Use of Metallized Cavities in Printed slot Arrays with Dielectric Substrates", IEEE Trans. Antenna Propagat., Vol. AP-35, May 1987.

[15]   J. T. Aberle and F. Zavosh, "Analysis of Probe-Fed Circular Microstrip Patches Backed by Circular Cavities", IEEE Trans. Electromagnetics, Vol. AP-14, 1994.

[16]   A. Henderson, J. R. James, and C. M. Hall, "Bandwidth Extension Techniques in Printed Conformal Antennas", Military Microwaves, Vol. MM 86, 198

[17]   D. M. Pozar and B. Kaufman, "Increasing the Bandwidth of a Microstrip Antenna by Proximity Coupling", Electrical Letters, Vol. 23, April 1987.

[18]   D. M. Pozar and D.H. Schaubert, "Scan Blindness in Infinite Phased Arrays of printed Dipoles", IEEE Trans. Antennas Propagat., Vol. AP-32, June 1984.

[19]   Indrasen Singh, Dr. V. S. Tripathi, "Microstrip Patch Antenna and its Application", Int. J. Comp. Tech. Appl., Vol 2(5), September 2011.

[20]   Ramesh Garg, Prakash Bartia, Inder Bahl, Apisak Ittipiboon, "Microstrip Antenna Design Handbook", Artech House Inc. Norwood, MA, 2001.

[21]   K. R. Carver and J. W. Mink, "Microstrip Antenna Technology", IEEE Trans. Antennas Propagat., Vol. AP-29, January 1981.

[22]   Y T Lo and S W Lee, "Antenna Handbook Theory, Applications & Design", Van Nostrand Rein Company, NY, 1997.

[23]   A. G. Derneryd, "Linearly Polarized Microstrip Antennas", IEEE Trans. Antennas Propagat., Vol. AP-24, November 1976.

The Impact of Big Data Analytics on Business Intelligence in E-Commerce: A Review

Shafkat M. Ibrahimy[1], and Ahmad I. Ibrahimy[2]

[1]Business School, University of Strathclyde, Glasgow, UK
[2]Dept. of Economics, University of Malaya, Kuala Lumpur, Malaysia

Corresponding author: dr.ahmad.ibrahimy@um.edu.my

Abstract— Big Data Analytics (BDA) is becoming a popular tool to gain insight into businesses and increase their competitive advantage. So, it is important to understand how it works and the opportunities it presents to growing businesses. The primary aim of this study is to evaluate the impact of using Data Analytics on Business Intelligence for e-commerce, focusing on how to promote the use of Big Data Analytics in the e-commerce sector by SMEs. One objective is to develop strategies that can be used by small businesses to take advantage of complicated tools such as BDA and sentiment analysis of social media platforms in order to boost their economic growth.

1. INTRODUCTION

Big Data Analytics (BDA) and Business Intelligence (BI) are becoming increasingly important tools in shaping the way e-commerce businesses make decisions (Mariani and Wamba, 2020). Using these tools aims for organisations to gain a competitive advantage within the growing e-commerce market by deploying effective strategies. Big data analytics is focused on uncovering why certain models work better than others by finding correlations and patterns. Its primary purpose is to use statistics and machine learning algorithms to answer specific questions by analysing data sets (Ertemel, 2015). On the other hand, business intelligence involves combining existing performance reports with information gained from data analytics to maximise profit (Ertemel, 2015). The widespread use of the Internet has led to the growth of customers utilising online shopping (e-commerce). More brands are spending their budget on creating an efficient online platform to meet customers' needs (Ferreira et al., 2017). Therefore, in the modern business climate, it has become more important for organisations to evaluate and process their performance data to identify what works and to create better marketing strategies that cater to their customers. According to Sun and Strang (2014), BI and analytics are being prioritised by nearly 50% of interviewed executives, and a further increase in its usage is expected in the next few years.

However, current studies investigating the use of analytics applied to business intelligence do not sufficiently address the consequence of applying these tools in utilising data from social media channels (Ram et al., 2016). This paper aims to gather and examine information to show how e-commerce businesses can gain an advantage by incorporating social media data and other possible data sources in conjunction with BI and big data analytics and evaluate its potential impact on the market. This study also proposes methods in which the use of BI and analytics can be further promoted for practical usage across businesses. The research objectives aim to answer the following:
1.   What is the impact of data analytics being applied to business intelligence in the e-commerce market?
2.   How can methods be developed to combine data from multiple sources, such as social media, for organisations to manage business intelligence?
3.   How can the use of big data analytics for BI be promoted for usage in smaller e-commerce businesses?

This research is important because of the relative difficulty in understanding data analytics and business intelligence, which can be further demystified for higher executives and managers (Zhuang et al., 2021). This

paper contributes by analysing the impact of data analytics within the context of business intelligence and synthesising methods to collect data from social media to develop marketing strategies for e-commerce businesses.

2. REVIEW OF LITERATURE

Data in the context of BDA can be defined by several qualities, including a large volume of data, speed in producing data and wide-ranging data types. Firstly, looking at volume, most of the existing data was produced in the last five years (Ertmel, 2015; Fan et al., 2015). With advancements in digital storage technology and reduced costs, collecting and storing such large volumes of data for BDA has become more feasible. Secondly, the speed of processing data in storage servers several years ago needed a significant amount of time. However, data can be analysed in real-time rapidly to make informed decisions (Fan et al., 2015). Lastly, for various data, structured and unstructured data are used in BDA to provide valuable insights (Ertmel, 2015). These data sources include financial statements, customer habits, inventory and other relevant variables relating to the business. According to Sun et al. (2015), there are three classification models of BDA, which are predictive, descriptive, and prescriptive analysis. Predictive analysis makes predictions by using existing data and statistics to look for patterns. Analysts use machine learning algorithms to build models that accurately forecast future changes. Statistical methods include linear regression, decision trees and neural networks. Its benefit is to reduce risks and increase operational efficiency. The descriptive analysis deals with trends and relationships dealing with traffic and customer engagement. Prescriptive analysis is focused on optimising solutions using various constraints and decision variables. It provides recommendations to optimize certain performance metrics while considering how it will also affect other metrics within the business, unlike predictive analysis, which mainly works with metrics in isolation.

Ferreira et al. (2017) note that Business Intelligence techniques are concerned with using internal and external information to get an overall picture of company performance. Typically, BI models generate key performance indicators (KPIs) and reports, allowing business executives to understand previously overlooked trends. By allocating more financial resources towards BI and using new technologically advanced tools, small businesses could get higher quality information that optimizes their assets. Several challenges exist in applying BI for e-commerce, which include the costs of creating good BI models, a lack of understanding of the impact of BI on profits that inhibit more businesses from using BI and the maintenance required. A solution is to identify important operational factors, including the number of monthly sales, product stock and daily visits.

To identify the factors that lead to promoting e-commerce activity, the Key Success Factors (KSF) can be introduced. Overall, KSF can be used to examine the expectations and motivations of online shoppers. Looking at online food stores, the primary reason shoppers buy online is to save time and better comfort (Colla and Lapoule, 2012). Online shopping allows customers to order products at any time of day conveniently. This makes it more accessible to customers with limited time during the day and accommodates those with disabilities. Negative factors include delivery time and lack of communication. In addition, customers may want assurance of the quality of products through close examination, which may deter them from using online shopping in preference to physically going to the store (Colla and Lapoule, 2012).

In line with other studies, a functional web design based on sound design principles and usable interfaces has been shown to guarantee the success of e-commerce operations (Colla and Lapoule, 2012). Several aspects of the website can be considered, such as having updated content (product information and deals) and the page's formatting, including layout, navigation buttons and quick feedback. E-commerce businesses need to allocate time to optimize their web pages' UX to make them more user-friendly. In addition, meeting customer needs by incorporating features such as having a search system capable of filtering through product lists and accurate images showcasing the product will help customers spend less time and make decisions about purchasing (Colla and Lapoule, 2012).

Additionally, the product storage and transport mode to the destination (customer) can be considered. One way is pick-up from the retail shop directly after orders, and the other is to send the package to the person's home or a selected designated location (owned by the retail store) where the person can come to pick up their deliveries at their convenience. The second option alleviates the risk of failure of not being able to receive packages while not at home, and it saves the business money (Colla and Lapoule, 2012). However, the second option is not as widely

used, so a strategy to promote this alternative method to more businesses should be considered. Another marketing strategy to increase engagement is for businesses to give complementary items to add competitive advantage and more value than their competition (Ferreira et al., 2017). Examining the impact of BDA on BI requires the identification of such key driving factors, which potentially correlate with customer satisfaction levels. Overall, looking at the various studies presented, offering various options to consumers tends to result in positive feedback. Considering the variables discussed above, big data analytics can be used to measure a correlation between user engagement and these variables to observe which factor has the most impact on profit. Later in the study, during the data collection stage, the factors mentioned can be asked about when interviewing e-commerce businesses to assess how organizations deal with driving engagement.

Regarding the architecture of incorporating business intelligence with the organization, an effective model will improve the business's competitive advantage and profits (Ferreira et al., 2017). One suggested architecture is modelled after Data Warehouse (Ferreira et al., 2017). The architecture supports the use of BI on four levels. The purpose of this architecture. The first level is the 'Data level', which involves the customer interacting with the online shopping website portal. Then, the data is collected and sent to a web server. This data is cleaned and made into logs or records to be extracted and transformed. The second level is the 'Data Warehouse Server'. It involves the company's Data Warehouse and data marts (a relational database to store records in rows and columns) to keep track of all the records. The third level is the 'OLAP Server'. At this level, data is arranged to be processed and analysed to identify the appropriate correlations or trends. Finally, at the fourth level is 'Business Intelligence Analytics'. At this level, after processing the data, reports are produced. The reports contain information on key drivers for change. Also, at this level, data mining techniques can be used for further evaluation (Ferreira et al., 2017).

3. METHODOLOGY

The methods used in this research will follow both a qualitative and semi-structured approach. A qualitative approach provides a more fluid understanding of the impact of BDA and BI by getting the perspective of business executives (Zhuang et al., 2021). The justification for conducting a qualitative study is as follows. According to Mariani and Wamba (2020), qualitative research allows for a deeper level of detail during analysis and can be adapted to the type of information streaming during collection. It makes it easier to change directions when the incoming data is not giving the desired outcomes, thus remaining less restricted. With qualitative research, when a common group is identified, gathering data from individuals within the group can be used to make predictions about the direction the group is likely to go in (Mariani and Wamba, 2020). In this study, the candidates belong to management-level executives of e-commerce businesses. In addition, qualitative research has the advantage of incorporating the human experience, which can potentially identify overlooked perspectives. Typically, the costs for this approach are reduced due to the smaller sample sizes, allowing the project to be conducted on a smaller budget. The results of a qualitative study are better suited for marketing departments to collaborate on ideas and make communication easier. A qualitative approach can be used to examine the relationship between customers and the brand by exploring the perspective of consumers.

The collection of data will be using primary sources of data. It will be gathered using semi-structured interviews of managers and employees working for several case businesses. The e-commerce businesses will span several types of industries, namely media and online retail services. The process will be divided into stages. The first stage is interviewing higher executives from two different teams with operations based in the UK. Also, at this stage, a few regular customers of those services will be interviewed. The first stage aims to gather preliminary data that will examine the extent to which BDA is used with BI in various contexts, and it will be used for comparisons later in the study. The second stage of interviews will be carried out after thoroughly examining the initially collected data and comparison with secondary data from other studies. After several months, a second set of interviews will involve the same candidates from the first stage and other candidates within the management team of multiple e-commerce businesses spanning different industries. This stage will allow the study to gain more data points and will be used to ask follow-up questions based on the first set of interviews (Mariani and Wamba, 2020). The contacts from the first set of interviews can provide a referral for further exploration during the second stage. In short, a qualitative study with semi-structured interviews for data collection is the desired approach to understand better the impact and challenges of BDA/BI used by businesses.

4. CONCLUSION

The topic to be discussed in this research is Big Data Analytics (BDA) applied in the E-Commerce sector, and it intends to focus on three main areas. First, how BDA and BI are impacting the e-commerce market's growth. Second, the aim is to recommend optimising BDA and BI usage by having a well-defined, integrated pipeline and using various data sources, such as social media. Third, to design methods in which the usage of BDA and BI can be promoted by small businesses for economic growth. This objective requires collecting primary data from businesses using a semi-structured approach for further analysis.

The research philosophy that will be followed is interpretivism. It is useful for interpreting qualitative data such as stakeholder perspective and behaviour. This study aims to identify common experiences faced by SMEs attempting to use BDA and BI as part of their pipeline. Interpretivism lines up with the study's objectives as it tries to understand and explore ways business's view BDA, and it allows the analysis to gain further insights by analysing different perspectives and user experiences in the context of e-commerce. The results of this study may be used to identify areas for improvement and make it easier to construct actionable strategies that SMEs can adopt to boost their economic growth. The results can reveal new valuable trends that exist within the e-commerce sector.

REFERENCES

[1] M. M. Mariani, and S. F.Wamba, "Exploring how consumer goods companies innovate in the digital age: The role of big data analytics companies," Journal of Business Research, Vol. 121, pp. 338-352, 2020.

[2] A. V. Ertemel,"Consumer insight as competitive advantage using big data and analytics" International Journal of Commerce and Finance, Vol. 1(1), pp. 45-51, 2015.

[3] T. Ferreira, I. Pedrosa, and J. Bernardino, "Business intelligence for e-commerce: Survey and research directions," Recent Advances in Information Systems and Technologies, Vol. 1(5), pp. 215-225. 2017.

[4] Z. Sun, and K. D. Strang, "Analytics service oriented architecture for enterprise information systems," In Proceedings of the 16th International Conference on information integration and web-based applications & services, pp. 508-516, 2014.

[5] J. Ram, C. Zhang, and A. Koronios, "The implications of big data analytics on business intelligence: A qualitative study in China," Procedia Computer Science, Vol. 87, pp. 221-226, 2016.

[6] W. Zhuang, M. C. Wang, I. Nakamoto, and M. Jiang, "Big data analytics in e-commerce for the US and China through literature reviewing," Journal of Systems Science and Information, Vol. 9(1), pp. 16-44, 2021.

[7] S. Fan, R. Y. Lau, and J. L. Zhao, "Demystifying big data analytics for business intelligence through the lens of marketing mix" Big Data Research, Vol. 2(1), pp. 28-32, 2015.

[8] Z. Sun, H. Zou, and K. Strang, "Big data analytics as a service for business intelligence," In Open and Big Data Management and Innovation: 14th IFIP WG 6.11 Conference on e-Business, e-Services, and e-Society, I3E 2015, Delft, The Netherlands, October 13-15, 2015, Proceedings 14 pp. 200-211, 2015. Springer International Publishing.

[9] E. Colla, and P. Lapoule, "E-commerce: exploring the critical success factors," International Journal of Retail & Distribution Management, Vol. 40(11), pp. 842-864, 2012.